TABLE 2. Survival of *Hipk1*$^{-/-}$ *Hipk2*$^{-/-}$ embryos during gestation[a]

Genotype	No. of live embryos (no. of embryos being resorbed) at indicated dpc:			
	8.5	9.5	10.5	12.5
Hipk1$^{-/-}$ *Hipk2*$^{+/+}$	7 (0)	34 (2)	22 (2)	14 (0)
Hipk1$^{-/-}$ *Hipk2*$^{+/-}$	12 (0)	43 (3)	30 (4)	23 (0)
Hipk1$^{-/-}$ *Hipk2*$^{-/-}$	5 (0)	24 (7)	12 (7)	1 (5)

[a] Mating type: *Hipk1*$^{-/-}$ *Hipk2*$^{+/-}$ × *Hipk1*$^{-/-}$ *Hipk2*$^{+/-}$.

as the incidence of NTD tends to be higher in females than in males (3, 35, 59). The incidence of NTD in the various *Hipk* mutants had not fully penetrated, even in the *Hipk1*$^{-/-}$ *Hipk2*$^{-/-}$ embryos, although the differences were significant and its penetrance was clearly affected by *Hipk* gene dosage (Table 3). For all genotypes, NTD occurred more frequently in females than in males. We also found that Hipk2 plays a more dominant role than Hipk1 in the suppression of NTD as well as in embryonic survival. Therefore, *Hipk1* and *Hipk2* mutations synergistically affect embryonic survival and neural tube closure.

Embryonic lethality in *Hipk1 Hipk2* double homozygotes involves p53. Female-skewed incidence of NTD has also been reported in *p53*-deficient mice, in which about 30% and 1% of homozygous females and males, respectively, exhibit exencephaly (59). Moreover, there is considerable evidence for functional interactions between HIPKs and p53 in human cells

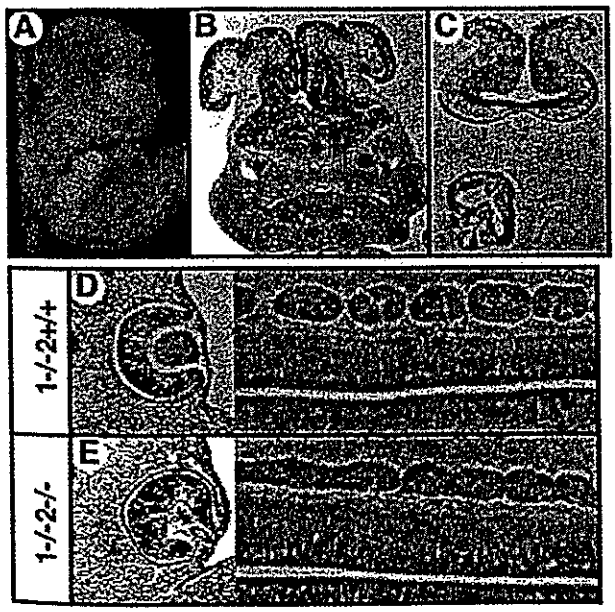

FIG. 3. Exencephaly and other histological abnormalities in *Hipk1*$^{-/-}$ *Hipk2*$^{-/-}$ embryos. (A) Lateral view of 11.5 dpc *Hipk1*$^{-/-}$ *Hipk2*$^{-/-}$ embryos exhibiting exencephaly. (B) Frontal section of 12.5 dpc *Hipk1*$^{-/-}$ *Hipk2*$^{-/-}$ embryos. (C) Frontal section of 9.5 dpc *Hipk1*$^{-/-}$ *Hipk2*$^{-/-}$ embryos. Overgrowth of neural tissue is usually confined to the region of the fore- and midbrain. (D) Normal formation of lens vesicle (left) and DRG (right) in *Hipk1*$^{-/-}$ *Hipk2*$^{+/+}$ embryos. (E) Failure of lens vesicle formation associated with disorientation of optic cups and fusion of DRGs in *Hipk1*$^{-/-}$ *Hipk2*$^{-/-}$ embryos.

TABLE 3. Incidence of NTD in male and female *Hipk* compound mutants

Genotype	Gender	NTD/total[a] (%)
Hipk1$^{-/-}$ *Hipk2*$^{+/+}$	Male	0/37 (0)
	Female	1/36 (2.8)
Hipk1$^{+/+}$ *Hipk2*$^{-/-}$	Male	0/23 (0)
	Female	1/21 (4.8)
Hipk1$^{+/-}$ *Hipk2*$^{+/-}$	Male	0/29 (0)
	Female	1/31 (3.2)
Hipk1$^{-/-}$ *Hipk2*$^{+/-}$	Male	1/62 (1.6)
	Female	5/63 (7.9)
Hipk1$^{+/-}$ *Hipk2*$^{-/-}$	Male	3/39 (7.7)
	Female	4/24 (16.7)
Hipk1$^{-/-}$ *Hipk2*$^{-/-}$	Male	11/28 (39.3)
	Female	10/18 (55.6)

[a] Number of embryos with NTD/total number of embryos with indicated genotype.

(12, 13, 14, 30, 39, 46, 57). These findings prompted us to address whether Hipks act via p53 during mouse development. Triple compound mutants were crossed to *Hipk1 Hipk2* compound mutants, and the morphology and genotype of the embryos were examined at 12.5 dpc. Four exencephalic embryos turned out to be *p53*$^{+/-}$ *Hipk1*$^{-/-}$ *Hipk2*$^{-/-}$, whereas none were *p53*$^{+/+}$ *Hipk1*$^{-/-}$ *Hipk2*$^{-/-}$; this result was surprising given the mating conditions, under which 4.5 embryos in the respective genotypes would have been expected. Although the number of samples examined was not sufficient to draw any statistical conclusions, it is possible that p53 is at least in part involved in the mediation of early embryonic lethality in *Hipk1*$^{-/-}$ *Hipk2*$^{-/-}$ embryos.

To address the molecular basis for this genetic interaction, we examined whether murine Hipk1 and Hipk2 were capable of acting together with murine p53 in the regulation of p53-dependent transcription. H1299 cells (p53$^{-/-}$) were cotransfected with expression vectors encoding human or murine p53 and murine Hipk1 or Hipk2 together with a reporter vector carrying the *p21*^{WAF1} or *Bax* promoter (Fig. 4). Both Hipk1 and Hipk2 increased p53-mediated transactivation of *p21*^{WAF1} and *Bax* promoters via murine p53 to an extent similar to that of the human counterpart. In contrast, Hipk1 or Hipk2 alone had no effect on either promoter. Therefore, Hipk1 and Hipk2 were shown to regulate p53 functions via physical interactions to mediate embryonic survival despite murine p53 lacking serine 46, which is conserved in human p53, phosphorylated by HIPK2, and involved in mediation of apoptosis upon genotoxic stimuli (14, 30, 47). Importantly, cotransfection of Hipk1 and Hipk2 did not exhibit any synergistic effects on the transactivation of p53 (Y. Li and A. Nakagawara, unpublished observations). Synergistic enhancement of respective single-mutant phenotypes in compound mutants might be due to functional redundancy or gene dosage effects rather than cooperation between Hipk1 and Hipk2.

Hipks mediate proliferation during neural and mesodermal development. In most mouse NTD models, NTDs reflect failure of neural fold elevation. Some NTD mutants, including *p53*, *Gadd45a*, and *Terc*, suggest that genes with a basic mitotic function also have a function specific to neural fold elevation (29, 34, 59). Indeed, HIPK family proteins have been shown to play significant roles in the regulation of cell growth and apop-

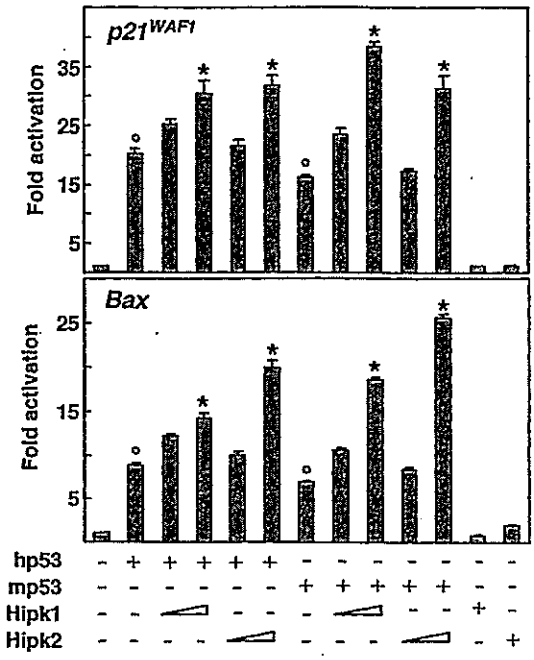

FIG. 4. Hipk1 and Hipk2 enhance p53-dependent transactivation of $p21^{WAF1}$ and *Bax* promoters via murine p53. p53-deficient H1299 cells were transiently cotransfected with the expression plasmid for human p53 (hp53) or murine p53 (mp53) along with luciferase reporter constructs containing $p21^{WAF1}$ (top) or *Bax* (bottom) promoter in the absence or presence of increasing amounts of transfected Hipk1 or Hipk2. Transfection efficiency was standardized against *Renilla* luciferase. The average relative luciferase activities in triplicate experiments are represented by bars. Means ± standard deviations of results are shown as fold induction of luciferase activity compared with number of cells transfected with vacant pcDNA3. Data shown are representative of three independent experiments with similar results. The significance of the differences were evaluated by the Student's *t* test. The bars marked with asterisks indicate significant difference ($P < 0.05$) from the bars indicated by open circles.

tosis in cultured cells and in primary sensory neurons (14, 15, 30, 39, 65). Therefore, we hypothesized that NTD in *Hipk1*$^{-/-}$ *Hipk2*$^{-/-}$ embryos may involve changes in cell growth in developing neural tube and paraxial mesoderm because the neural tube closure involves not only the neuroectoderm but also the underlying paraxial mesoderm. We first examined cellular proliferation by labeling 9.5 dpc embryos by BrdU around the level of midbrain/hindbrain boundary and prospective cervicothoracic boundary. We crossed *Hipk1*$^{-/-}$ *Hipk2*$^{+/-}$ mice and compared *Hipk1*$^{-/-}$ *Hipk2*$^{+/+}$ and *Hipk1*$^{-/-}$ *Hipk2*$^{-/-}$ embryos because *Hipk1* single mutants were morphologically normal. In the cranial region, the frequency of mitotic cells in the *Hipk1*$^{-/-}$ *Hipk2*$^{-/-}$ neural tube was significantly reduced to 45% and 29% of that of the *Hipk1*$^{-/-}$ embryos in the dorsal and ventral regions, respectively (Fig. 5A, B, E, F, and I). Proliferation of the cephalic mesoderm of the *Hipk1*$^{-/-}$ *Hipk2*$^{-/-}$ embryos was also reduced to 43% of the *Hipk1*$^{-/-}$ embryos. In the trunk region, proliferation was affected in the ventral but not the dorsal region of the neural tube and in the sclerotomal compartment of the paraxial mesoderm in the *Hipk1*$^{-/-}$ *Hipk2*$^{-/-}$ embryos (Fig. 5C, D, G, H, and J). We next investigated the frequency of apoptotic cells in the *Hipk1*$^{-/-}$ *Hipk2*$^{+/+}$ and *Hipk1*$^{-/-}$ *Hipk2*$^{-/-}$ embryos by TUNEL staining. Although we did not see a significant difference within the neural tube in the cranial region, numbers of apoptotic cells were significantly increased in the condensing trigeminal and facioacoustic neural crest cells (Fig. 5K). In the trunk region, we reproducibly observed more apoptotic outbursts in the sclerotomal compartment in *Hipk1*$^{-/-}$ *Hipk2*$^{-/-}$ than *Hipk1*$^{-/-}$ *Hipk2*$^{+/+}$ embryos but did not see significant changes in the neural tube. Therefore, Hipks are shown to promote mitosis and repress apoptotic outbursts in a tissue-specific manner during embryogenesis, which could partly be the cause of the defects in neural fold elevation. Interestingly, the fusion of DRGs is caused by an insufficient proliferation of sclerotomal cells, which may fail to provide the mesenchymal cells that separate DRGs, or by defects in craniocaudal specification of the somitic mesoderm (50, 58, 62). Craniocaudal specification and subsequent segmentation of the somites occurs normally, as revealed by the expression of *Uncx4.1* and *Hes5* in *Hipk1*$^{-/-}$ *Hipk2*$^{-/-}$ embryos (K. Isono, unpublished). Therefore, DRG fusion may also be at least in part due to impaired proliferation of sclerotomal cells.

Defective *Pax1* induction by Shh in *Hipk* double mutants. We next examined the expression of genes involved in the incidence of NTD in *Hipk1*$^{-/-}$ *Hipk2*$^{-/-}$ embryos. It is particularly interesting to investigate the expression of *Twist*, *Shh*, and Shh-dependent genes like *Pax1* and *Pax3* (5, 6, 22). Cranial NTD in *Twist* homozygotes was associated with the reduction of proliferation and expansion of the cranial mesenchyme. Shh is a predominant signaling molecule involved in neural fold elevation, which mediates the proliferation and differentiation of the neural tube and paraxial mesoderm by inducing a series of transcriptional regulators in the ventral regions of the respective tissues (22, 56). We further examined the expression of *Pax1*, which is expressed in the sclerotome in a Shh-dependent manner and is involved in the mediation of the proliferation of sclerotomal cells (22, 62). NTD in the *Pax3* mutant was shown to involve p53, and *Pax3* expression is repressed in the ventral region of the neural tube and paraxial mesoderm by Shh (20, 49).

In the wild-type and *Hipk1*$^{-/-}$ embryos at 9.5 dpc, *Twist* is expressed in the branchial arches and paraxial and lateral plate mesoderm (Fig. 6A, left). In *Hipk1*$^{-/-}$ *Hipk2*$^{-/-}$ embryos, the expression was significantly reduced in the paraxial and lateral plate mesoderms but not in the branchial arches (Fig. 6A, right). *Shh* expression was not significantly changed in the notochord of *Hipk1*$^{-/-}$ *Hipk2*$^{-/-}$ embryos but was reduced in the floor plate (Fig. 6B, bottom). Sclerotomal expression of the *Pax1* gene was decreased in *Hipk1*$^{-/-}$ *Hipk2*$^{-/-}$ embryos while the expression in the pharyngeal pouches was not significantly changed (Fig. 6B, top). The expression of *Pax3* in the dorsal regions of fore-, mid-, and hindbrain was not grossly changed in *Hipk1*$^{-/-}$ *Hipk2*$^{-/-}$ embryos irrespective of exencephaly (K. Isono, unpublished). However, we observed that in the neural tube in *Hipk1*$^{-/-}$ *Hipk2*$^{-/-}$ embryos, the *Pax3* expression domain was ventrally expanded (Fig. 6C). Since the expression of *Pax1* and *Pax3* in the paraxial mesoderm and/or neural tube are regulated by Shh, it is likely that Shh signaling is affected in *Hipk1*$^{-/-}$ *Hipk2*$^{-/-}$ embryos. To exclude the possibility that the expression of Shh gene products is reduced in double homozygotes, we monitored the expression of *Foxa2* in the floor plate, which is also Shh dependent (56) (Fig. 6D). *Foxa2*

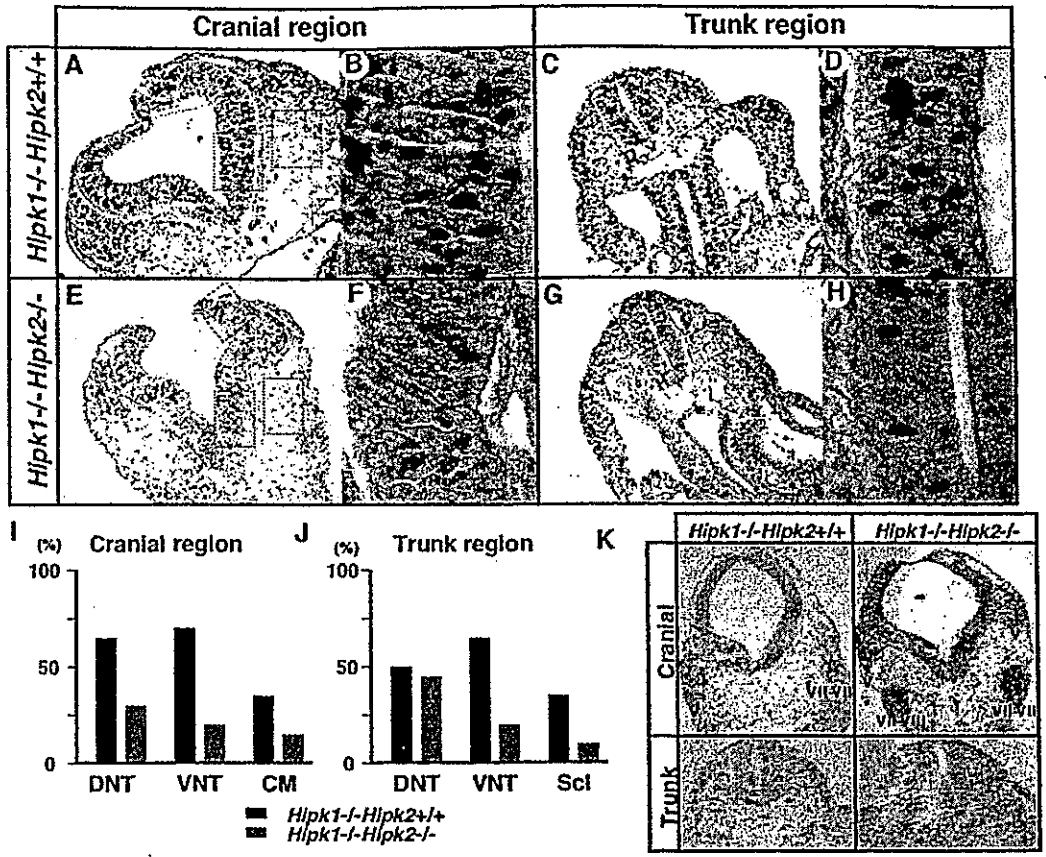

FIG. 5. Reduced mitotic cells and increased apoptotic cells in *Hipk1*$^{-/-}$ *Hipk2*$^{-/-}$ embryos. (A) Distribution of BrdU-positive cells in the cranial region of *Hipk1*$^{-/-}$ *Hipk2*$^{+/+}$ embryos at 9.5 dpc. Frequencies of BrdU-labeled cells were counted in the boxes in the dorsal region of the neural tube (DNT in panels I and J), ventral region of the neural tube (VNT in panels I and J, with a higher magnification shown in panel B) and cephalic mesoderm (CM in panels I and J). (B) Higher magnification of the area indicated by box B in panel A. (C) Distribution of BrdU-positive cells in the prospective trunk regions of *Hipk1*$^{-/-}$ *Hipk2*$^{+/+}$ embryos at 9.5 dpc. Frequencies of BrdU-labeled cells were counted in the boxes in the dorsal region of the neural tube (DNT in panels I and J), ventral region of the neural tube (VNT in panels I and J, with a higher magnification shown in panel D) and sclerotome (Scl in panels I and J). (D) Higher magnification of the area indicated by box D in panel C. (E) Distribution of BrdU-positive cells in the cranial regions of *Hipk1*$^{-/-}$ *Hipk2*$^{-/-}$ embryos at 9.5 dpc. The frequency of BrdU-labeled cells was counted in the areas demarcated by the boxes. (F) Higher magnification of the area indicated by box F in panel E. (G) Distribution of BrdU-positive cells in the prospective interlimb regions of *Hipk1*$^{-/-}$ *Hipk2*$^{-/-}$ embryos at 9.5 dpc. (H) Higher magnification of the area indicated by box H in panel G. (I) Frequency of BrdU-labeled cells in the regions indicated by boxes in the cranial region. DNT, dorsal region of the neural tube; VNT, ventral region of the neural tube; CM, cephalic mesoderm. Means are shown by black (*Hipk1*$^{-/-}$ *Hipk2*$^{+/+}$) and gray (*Hipk1*$^{-/-}$ *Hipk2*$^{-/-}$) bars. (J) Frequency of BrdU-labeled cells in the regions indicated by boxes in the prospective trunk region. Scl, sclerotome. (K) Distribution of apoptotic cells revealed by TUNEL staining in the cranial (top) and prospective trunk (bottom) regions. In the cranial region, sections through the trigeminal (V) and facioacoustic (VII-VIII) neural crest tissues are shown although the section of *Hipk1*$^{-/-}$ *Hipk2*$^{+/+}$ embryo (top left) is oblique. Note the significant apoptotic outbursts in the trigeminal and facioacoustic neural crest tissues of the *Hipk1*$^{-/-}$ *Hipk2*$^{-/-}$ embryo (top right). In the prospective trunk region, apoptotic outbursts are more pronounced in the sclerotomal compartments in the *Hipk1*$^{-/-}$ *Hipk2*$^{-/-}$ embryo (bottom right) than the *Hipk1*$^{-/-}$ *Hipk2*$^{+/+}$ embryo (bottom left).

expression was not changed in the floor plate or the midgut endoderm. Therefore, it is likely that the notochordal expression of Shh protein is unaffected in *Hipk1*$^{-/-}$ *Hipk2*$^{-/-}$ embryos. To examine whether cellular responses might be primarily impaired upon Shh signaling, we cultured explants of unsegmented paraxial mesoderm, as described previously, in the presence of Shh and investigated the *Pax1* expression in *Hipk1*$^{-/-}$ *Hipk2*$^{-/-}$ embryos (20, 21). Shh clearly induced *Pax1* expression in the micromass culture of wild-type presomitic mesoderm (Fig. 6E, left). In contrast, Shh-dependent expression of *Pax1* was totally abolished in the paraxial mesoderm derived from *Hipk1*$^{-/-}$ *Hipk2*$^{-/-}$ embryos (Fig. 6E, right), suggesting that Shh signaling to the *Pax1* induction was impaired. The expression of *Twist* was also reduced to about half that of the wild type. We did not see a significant reduction of *Pax1* expression in either single mutant (H. Koseki, unpublished). Therefore, it is likely that Hipk1 and Hipk2 are involved in the mediation of Shh-dependent proliferation of the paraxial mesoderm at least in part via transcriptional regulation of *Pax1* (6, 22).

Regulation of *Hox* gene expression by Hipks. HIPK1 and HIPK2 are capable of binding to the homeodomains of not only NK classes but also *Hox* cluster genes (37). Evidence for autoregulation of *Hoxa4* and *Drosophila Deformed* (4, 48) suggested the involvement of Hipks in the expression of *Hox* genes. This possibility was further supported by the following

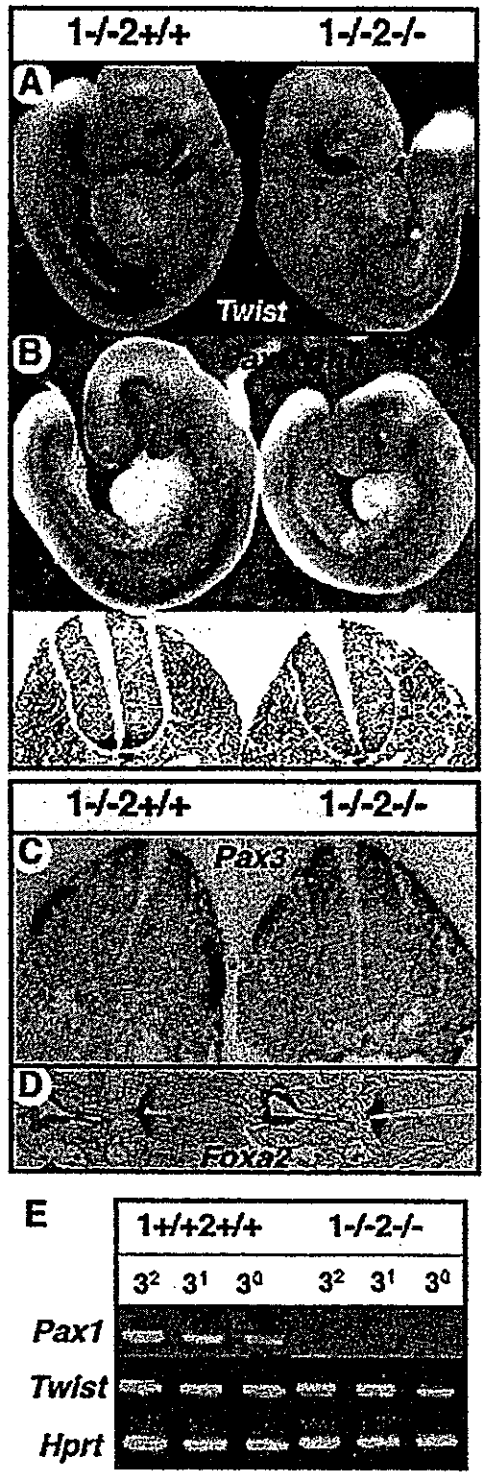

FIG. 6. Changes in Shh-dependent gene expression in the paraxial mesoderm and neural tube of *Hipk1*$^{-/-}$ *Hipk2*$^{-/-}$ embryos. (A) Expression of *Twist* in *Hipk1*$^{-/-}$ *Hipk2*$^{+/+}$ (left) and *Hipk1*$^{-/-}$ *Hipk2*$^{-/-}$ (right) embryos at 9.5 dpc. (B) Expression of *Pax1* and *Shh* in *Hipk1*$^{-/-}$ *Hipk2*$^{+/+}$ (left) and *Hipk1*$^{-/-}$ *Hipk2*$^{-/-}$ (right) embryos at 9.5 dpc. Whole-mount in situ hybridization (top) revealed significant reduction of Pax1 expression in *Hipk1*$^{-/-}$ *Hipk2*$^{-/-}$ (top right). Sections of the prospective cervical regions are shown (bottom). (C) Expression of *Pax3* in the prospective cervical regions of *Hipk1*$^{-/-}$ *Hipk2*$^{+/+}$ (left) and *Hipk1*$^{-/-}$ *Hipk2*$^{-/-}$ (right) embryos at 9.5 dpc. (D) Expression of *Foxa2* at the midgut level of *Hipk1*$^{-/-}$ *Hipk2*$^{+/+}$ (left) and *Hipk1*$^{-/-}$ *Hipk2*$^{-/-}$ (right) embryos at 9.5 dpc. (E) Impaired *Pax1* induction by Shh in explant culture of presomitic mesoderm from 9.5 dpc *Hipk1*$^{-/-}$ *Hipk2*$^{-/-}$ embryos. Total RNA extracted from the explant culture of presomitic mesoderm from wild-type (left) and *Hipk1*$^{-/-}$ *Hipk2*$^{-/-}$ (right) embryos were reverse transcribed and subjected to PCR for *Pax1* and *Twist*, with *hprt* used as a control.

observations. CRE-binding protein, which interacts with Hipk2, was shown to be involved in the regulation of *Hox* gene expression via binding to the *Hox* gene promoters (54). Furthermore, Hipk2 was demonstrated to be activated by Wnt signaling, which was also shown to impact *Hox* gene expression, in cultured cells (36, 41). Therefore, we examined the expression of *Hox* genes and the anterior-posterior specification of the axial skeleton in *Hipk* mutants. Sixty-nine and 20% of *Hipk1*$^{-/-}$ *Hipk2*$^{+/-}$ and *Hipk1*$^{+/-}$ *Hipk2*$^{-/-}$ mice, respectively, possessed ectopic ribs associated with the seventh cervical vertebra (C7) and missed the prominent spinous process from the second thoracic vertebra (T2), which may represent posterior transformations around the cervicothoracic boundary (Fig. 7A and B). The ectopic ribs were present in the single homozygotes with lower penetrance, whereas there were no changes in single heterozygotes (Fig. 7C). Therefore, Hipk1 and Hipk2 synergistically regulate the segmental identity. Next, we examined the *Hox* gene expression in the paraxial mesoderm and neural tube. In the paraxial mesoderm, no obvious changes were observed in *Hoxb6* or *Hoxb8* expression, which demarcates the prospective cervicothoracic boundary, in 11.5 dpc *Hipk1*$^{-/-}$ *Hipk2*$^{-/-}$ embryos (H. Koseki, unpublished). We went on to analyze the expression of *Hox* genes at 9.5 dpc, particularly in the neural tube. *Hoxb1* is predominantly expressed in rhombomere 4 (r4) and in the prospective spinal cord in the wild type (Fig. 7D). We found groups of *Hoxb1*-expressing cells in the r6 region in *Hipk1*$^{+/-}$ *Hipk2*$^{+/-}$ and *Hipk1*$^{-/-}$ *Hipk2*$^{-/-}$ embryos (Fig. 7E and F). The *Hoxb6* expression in the dorsal neural tube was seen up to the level of the fourth myotome in the wild type (Fig. 7G). This expression was extended to the level of the third myotome in *Hipk1*$^{-/-}$ *Hipk2*$^{-/-}$ embryos (Fig. 7H). In contrast, the expression of *Hoxa1*, *Hoxa2*, or *Hoxb3* was not changed in *Hipk1*$^{-/-}$ *Hipk2*$^{-/-}$ embryos (K. Isono, unpublished). Therefore, this suggests that Hipk1 and Hipk2 regulate the expression of a subset of *Hox* cluster genes during embryogenesis. It is possible that derepression of *Hox* expression in *Hipk* compound mutants may involve an interaction between Hox proteins and Hipk gene products. Otherwise, considering that Hipks act as repressors with histone deacetylase complexes (7, 37), Hipk1 and Hipk2 might regulate *Hox* expression at the transcription level. Whatever the intrinsic mechanisms that operate to maintain *Hox* gene expressions, *Hox* gene expressions are known to be regulated by various morphogenetic signals that include Wnts, retinoic acids, Notch signals, fibroblast growth factors, and maybe others (10, 41, 67). Derepression of *Hox* cluster genes in *Hipk* mutants might be another indication for the role of Hipks to integrate various signals and mediate appropriate cell growth to accomplish normal organ development.

The role of Hipks for activation of cell cycle checkpoints in embryonic cells. Previous studies using human tumor cell lines

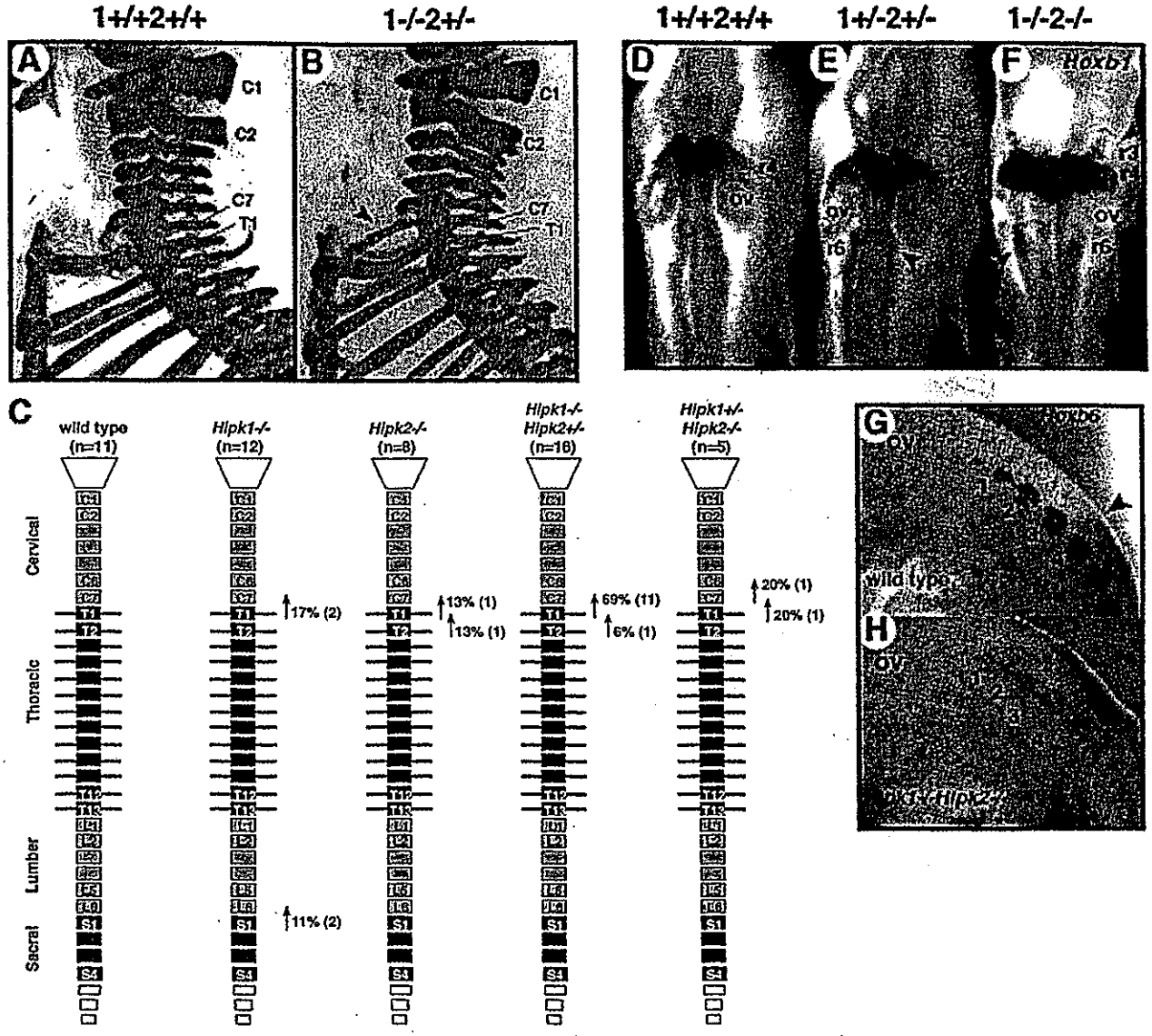

FIG. 7. Homoeotic transformations of the axial skeleton and ectopic expressions of *Hoxb1* and *Hoxb6* in the neural tubes of *Hipk1*$^{-/-}$ *Hipk2*$^{-/-}$ embryos. (A) Lateral view of the cervicothoracic region of a newborn *Hipk1*$^{+/+}$ *Hipk2*$^{+/+}$ mouse. Abbreviations: C1, first cervical vertebra; C2, second cervical vertebra; C7, seventh cervical vertebra; T1, first thoracic vertebra. (B) Lateral view of the cervicothoracic region of a newborn *Hipk1*$^{-/-}$ *Hipk2*$^{-/-}$ mouse. An ectopic rib associated with C7 is indicated by the blue arrowhead. (C) Summary of homoeotic transformations of axial skeleton. The numbers of affected individuals are shown in parentheses. T1→C7 transformation is characterized by the ectopic rib associated with C7. T2→T1 transformation is characterized by the shift of the prominent spinous process from T2 to T1. C7→C6 transformation is characterized by the lack of anterior processes from C6 and the concomitant appearance of the anterior process on C5. S1→L6 transformation is characterized by the sacroiliac joint in L6. (D) Expression of *Hoxb1* in *Hipk1*$^{+/+}$ *Hipk2*$^{+/+}$ embryos at 9.5 dpc. Note that the expression is localized to rhombomere 4 (r4) and the prospective spinal cord. ov, otic vesicle. (E) Expression of *Hoxb1* in *Hipk1*$^{+/-}$ *Hipk2*$^{+/-}$ embryos at 9.5 dpc. Note the subtle derepression in rhombomere 6 (r6), which is indicated by an arrowhead. (F) Expression of *Hoxb1* in *Hipk1*$^{-/-}$ *Hipk2*$^{-/-}$ embryos at 9.5 dpc. Note the derepression in rhombomere 3 (r3) and r6, which are indicated by arrowheads. (G) Expression of *Hoxb6* in *Hipk1*$^{+/+}$ *Hipk2*$^{+/+}$ embryos at 9.5 dpc. Positions of somites are visualized by *myogenin* expression, and each segment is numerically indicated. The anterior boundary of *Hoxb6* expression in the neural tube is indicated by an arrowhead. (H) Expression of *Hoxb6* in *Hipk1*$^{-/-}$ *Hipk2*$^{-/-}$ embryos at 9.5 dpc. Note that the anterior boundary is shifted to the level of the third somite.

have shown that HIPK1 and HIPK2 were involved in mediating DNA damage-induced apoptosis or cell cycle arrest by regulating the p53 and/or CtBP (14, 30, 38, 68, 69). If this is also the case in primary embryonic cells, it is hypothesized that Hipk1 and Hipk2 are involved in eliminating proliferating progenitors with genetic instability, which may in turn guarantee normal organ development and homeostasis. We therefore examined cellular growth upon genotoxic insult by using proliferating primary MEFs generated from 12.5 dpc fetuses, apart from the double homozygotes, which die at an earlier stage. We tested the UV response of MEFs with mutations in *Hipk* and p53$^{-/-}$, as a reference. The numbers of dead and living cells were counted 6, 11, and 24 h after UV (50 J/m^2) exposure. *Hipk1* and *Hipk2* single-mutant MEFs were slightly

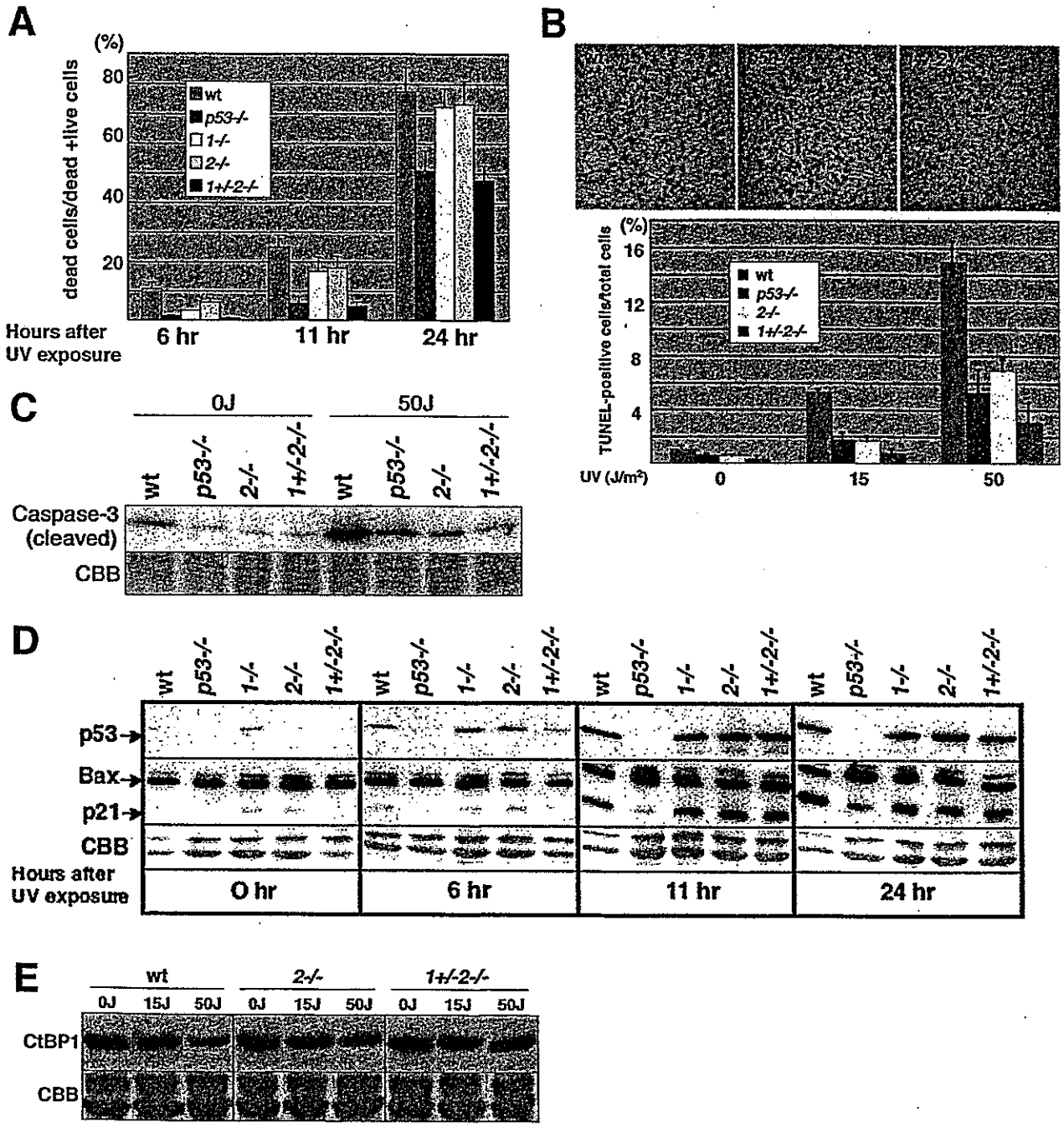

FIG. 8. Hipks mediate UV-induced apoptosis in primary MEFs. (A) Frequency of dead cells 6, 11, and 24 h after UV irradiation as revealed by trypan blue exclusion. Means ± standard deviations are shown by bars for the respective genotypes. (B) Frequency of apoptotic cells 12 h after UV irradiation (15 or 50 J/m^2) as revealed by TUNEL assay. (Top) Microscopic views of TUNEL-positive cells induced by UV (15 J/m^2) in wild-type (wt; left), *p53*$^{-/-}$ (middle), and *Hipk1*$^{+/-}$ *Hipk2*$^{-/-}$ (right) MEFs. (Bottom) Frequency of apoptotic cells 12 h after UV irradiation (15 or 50 J/m^2) are summarized. Means ± standard deviations are shown by bars for the respective genotypes. (C) Western blot analyses for the cleaved form of caspase-3 in MEFs with respective genotypes. Nonirradiated MEFs were used as the 0 J control. (D) Expression of p53, Bax, and p21^{WAF1} in *Hipk* mutant MEFs 6, 11, and 24 h after UV irradiation. Nonirradiated MEFs were used as the 0 h control. After immunodetection, membranes were stained with Coomassie brilliant blue (CBB) to quantify the amounts of blotted proteins. (E) Expression of CtBP1 in *Hipk* mutant MEFs 12 h after UV irradiation (15 or 50 J/m^2).

resistant to UV exposure compared to the wild type (Fig. 8A). *Hipk1*$^{+/-}$ *Hipk2*$^{-/-}$ MEFs were more resistant than single mutants, and the frequency of dead cells was equivalent to that for *p53*$^{-/-}$ cells. This result was further confirmed by TUNEL assay and Western blotting for cleaved caspase-3, which represents apoptotic outbursts. Frequency of TUNEL-positive cells induced by UV irradiation was significantly reduced in *p53*$^{-/-}$, *Hipk2*$^{-/-}$, and *Hipk1*$^{+/-}$ *Hipk2*$^{-/-}$ MEFs compared to

the wild type (Fig. 8B). Concordantly, accumulation of cleaved caspase-3 upon UV irradiation was affected in *p53*$^{-/-}$, *Hipk2*$^{-/-}$, and *Hipk1*$^{+/-}$ *Hipk2*$^{-/-}$ MEFs (Fig. 8C). In conclusion, Hipk1 and Hipk2 were required to mediate apoptosis upon UV stress in murine proliferating MEFs as well as human tumor cell lines. Therefore, Hipks were suggested to activate cell cycle checkpoints in embryonic primary cells.

We next addressed whether the p53 or CtBP pathway was activated by Hipk1 and Hipk2 upon UV irradiation in MEFs. In UV-irradiated human tumor cells, HIPK2 activates human p53 at least via phosphorylation of serine 46, which in turn induces the apoptosis-inducible factor gene *p53AIP1* (14, 30, 47). Hipks were shown to activate murine p53-mediated transcription of *p21*^{WAF1} and *Bax* promoters, and p53 was suggested to mediate embryonic lethality in *Hipk1 Hipk2* double homozygotes (Fig. 4). However, murine p53 does not possess a serine residue equivalent to the serine 46 of human p53, and neither has a *p53AIP1* locus been found in the mouse genome (see Fig. S1 and S2 in the supplemental material). We thus examined the involvement of p53 by analyzing the expression of p53 and the two p53 targets, p21^{WAF1} and Bax, in *Hipk* mutants upon UV irradiation (18, 43). Interestingly, we did not see a significant difference in the expression of p53, p21^{WAF1}, or Bax between *Hipk* mutants and the wild type (Fig. 8D). We then examined the cellular senescence in *Hipk*-mutated MEFs since this is accompanied by accumulation of p53 gene products and cancelled by *p53* mutation (27). *Hipk1*$^{+/-}$ *Hipk2*$^{-/-}$ and *Hipk1*$^{-/-}$ *Hipk2*$^{+/-}$ MEFs senesced like the wild type in a strict 3T9 protocol while *p53*$^{-/-}$ MEFs kept on growing (K. Isono, unpublished) (27). Therefore, Hipk1 and/or Hipk2 may not mediate apoptosis or cellular senescence upon UV or mitotic stress, respectively, by stabilizing p53. However, we could not exclude other possibilities that Hipk1 and Hipk2 might activate p53 through phosphorylation of other common residues or other modifications.

We went on to analyze the expression of CtBP in *Hipk* mutant MEFs, since UV-inducible phosphorylation of human CtBP at serine 422 by HIPK2 destabilizes CtBP and the reduction of CtBP promotes apoptosis irrespective of p53 activation (68, 69). In the wild-type MEFs, UV irradiation induced a reduction of CtBP1 expression in a UV dose-dependent manner (Fig. 8E). In contrast, CtBP1 expression was not significantly decreased after UV exposure in *Hipk1*$^{+/-}$ *Hipk2*$^{-/-}$, *Hipk1*$^{-/-}$, or *Hipk2*$^{-/-}$ MEFs. Therefore, it is likely that Hipk1 and Hipk2 are involved in mediating UV-induced apoptosis by decreasing CtBP expression in MEFs, although it might be of note that the stabilized CtBP level alone cannot explain the difference of apoptotic resistance between each *Hipk* single mutant and *Hipk1*$^{+/-}$ *Hipk2*$^{-/-}$. Taken together, Hipk1 and Hipk2 are required for not only proliferation of embryonic cells upon morphogenetic signals but also activation of cell cycle checkpoints upon genotoxic stimulus during embryogenesis.

DISCUSSION

In this study, by using *Hipk1 Hipk2* compound mutants, we have shown that Hipk1 and Hipk2 act in synergy to mediate growth regulation upon morphogenetic and genotoxic signals. Since both *Hipk1* and *Hipk2* are expressed almost ubiquitously around 9.5 dpc and their products are coexpressed in the nuclei of MEFs and colocalized to subnuclear domains following overexpression, the molecular basis for this synergy is most likely due to the functional overlap between Hipk1 and Hipk2 and mutually compensative properties, although Hipk2 may exert a slightly dominant role. It is also noteworthy that embryonic survival and neural tube closure are affected in compound mutants in a gene dosage-dependent manner. This genetic interaction could imply that the total amount of Hipk protein is an important parameter in mediating the appropriate cellular responses required for normal development. Indeed, the expression level of HIPK2, which correlates in a linear fashion with the degree of DNA damage, differentially impacts the posttranslational modifications of human p53 and subsequent cellular responses (12, 13). It has also been shown that the phosphorylation and sumoylation statuses of HIPK2 are altered by various cellular inputs, which in turn affect the HIPK2 functions (32, 60). It is therefore likely that several distinct mechanisms operate to maintain the functional quantity of Hipks. In vertebrates, the presence of three structurally and functionally homologous Hipk proteins might be involved in guaranteeing that the appropriate amounts of functional Hipks are available throughout embryogenesis and in allowing postnatal survival.

Regulation of cell growth by Hipk1 and Hipk2 during embryogenesis is shown to involve not only induction of transcription factors required for morphogenetic proliferation but also activation of cell cycle checkpoints upon genotoxic stimulation. It is thus possible that activation of Hipks by various morphogenetic signals may sensitize proliferating progenitor cells for apoptotic outbursts, which may facilitate elimination of cells with genetic instability. Notably, loss of Hipks also activates checkpoints since embryonic lethality in *Hipk1*$^{-/-}$ *Hipk2*$^{-/-}$ embryos is at least partly alleviated by *p53* mutation. Therefore Hipks are tightly linked to cell cycle checkpoint mechanisms in embryonic cells and may either activate or repress their functions to mediate the appropriate cellular responses by sensing various extracellular stimuli.

It has been suggested that, by regulating the transcription of target genes such as *Pax1* and *Pax3*, Hipks mediate Shh signaling, which results in the proliferation in developing paraxial mesoderm and neural tube. This is in agreement with previous observations that HIPKs bind and activate CRE-binding protein, which is a functional component of Shh signaling (2, 9, 22). Intriguingly, HIPK2 has also been shown to negatively regulate BMP-induced transcription by inhibiting Smads (26). Since opposing long-range signals mediated by Shh and BMP4 are essential for dorsoventral specification of the neural tube and paraxial mesoderm (22, 42), Hipks may be involved in the integration of two antagonizing signals and thereby facilitate cell growth and differentiation in the ventral regions. Different cellular inputs appear to induce different modifications or alter the subcellular localization of Hipks and subsequently drive transcription of different target genes by means of differential interactions with its binding partners (60). This previous conclusion is supported by our findings that Hipk1 and Hipk2 promote UV-induced apoptosis in MEFs but repress apoptotic outbursts in some differentiating tissues. The most attractive scenario for this integrating role of Hipks during the dorsoventral specification is that a certain alteration of Hipks in-

duced by Shh signaling may facilitate the formation of a repressive complex with Ski and Smads, which may in turn inhibit the BMP4 signaling cascade. Previous studies have demonstrated that HIPKs were capable of responding to a vast range of extracellular signals (60). It is possible that Hipks may play this integrating role during the induction and/or maintenance of *Hox* gene expressions, which are mediated by a combination of various signaling molecules including at least Wnts, retinoic acid, Notch, and fibroblast growth factors (10, 41, 67). Taken together, Hipks integrate these signals in order to mediate between the appropriate growth responses during development and cellular homeostasis. It is notable that functional coupling has recently been found between the differentiation checkpoint mechanism and genotoxic signaling cascade during myogenesis and that this contributes to differentiation of muscle precursors (53). Hipks could be involved in the qualification of stressed cells by various extracellular inputs, which would secure the cells' further development and survival.

NTDs, particularly exencephaly and spina bifida, are common human birth defects, and their genetics are very complex. Accordingly, in mice, mutations at many loci have been shown to cause NTDs (35). The present study clearly indicated the protective roles of Hipks against NTD, particularly exencephaly. In nearly all known NTD mutants examined, NTD arises from a failure to complete the process of elevation of the neural folds to become vertical. Neural fold elevation has been shown to be dependent on the proliferation of the neural fold and/or the underlying mesoderm because reduced mitosis in these tissues is associated with NTDs in *Twist*, *Pax1/PDGFRα*, *Pax1/foxc2*, *Shh*, and *Opb* mutants (5, 6, 17, 23, 28). It is therefore likely that Hipks mediate neural fold elevation by regulating mitosis in the neural folds and/or underlying mesoderm, which may involve the Shh signaling cascade (66). It is also noteworthy that mutations in genes encoding interacting partners for Hipks, including *p53*, *Cbp*, *Axin*, and *Ski*, have been shown to cause exencephaly (35). Importantly, these have also been shown to be involved in the signaling cascades of Shh, Wnt, or BMPs (2, 8, 9, 26, 57, 61). Therefore, in conclusion, it is hypothesized that coordination of the proliferation in the subdomains of neural tube and paraxial mesoderm is required for correct neural fold elevation and that Hipks could be involved in the coordination of the mitotic responses to various morphogenetic signals (66).

ACKNOWLEDGMENTS

This project was supported by Special Coordination Funds for the Promotion of Science and Technology from the Ministry of Education, Culture, Sports, Science and Technology of the Japanese Government (H.K.).

We thank Ryoko Moriizumi, Sanae Takeda, Misao Uchida, Tamie Endo, and the late Shozo Sugimori for their help.

REFERENCES

1. Akasaka, T., M. Kanno, R. Balling, M. A. Mieza, M. Taniguchi, and H. Koseki. 1996. A role for Mel18, a Polycomb group-related vertebrate gene, during the anteroposterior specification of the axial skeleton. Development 122:1513–1522.
2. Akimaru, H., Y. Chen, P. Dai, D. X. Hou, M. Nonaka, S. M. Smolik, S. Armstrong, R. H. Goodman, and S. Ishii. 1997. Drosophila CBP is a co-activator of cubitus interruptus in hedgehog signalling. Nature 386:735–738.
3. Armstrong, J. F., M. H. Kaufman, D. J. Harrison, and A. R. Clarke. 1995. High-frequency developmental abnormalities in p53-deficient mice. Curr. Biol. 5:931–936.
4. Bergson, C., and W. McGinnis. 1990. An autoregulatory enhancer element of the Drosophila homeotic gene Deformed. EMBO J. 9:4287–4297.
5. Chen, Z. F., and R. R. Behringer. 1995. *Twist* is required in head mesenchyme for cranial neural tube morphogenesis. Gene Dev. 9:689–699.
6. Chiang, C., Y. Litingtung, E. Lee, K. E. Young, J. L. Corden, H. Westphal, and P. A. Beachy. 1996. Cyclopia and defective axial patterning in mice lacking Sonic hedgehog gene function. Nature 383:407–413.
7. Choi, C. Y., Y. H. Kim, H. J. Kwon, and Y. Kim. 1999. The homeodomain protein NK-3 recruits Groucho and a histone deacetylase complex to repress transcription. J. Biol. Chem. 274:33194–33197.
8. Cordenonsi, M., S. Dupont, S. Maretto, A. Insinga, C. Imbriano, and S. Piccolo. 2003. Links between tumor suppressors: p53 is required for TGF-beta gene responses by cooperating with Smads. Cell 113:301–314.
9. Dai, P., H. Akimaru, Y. Tanaka, T. Maekawa, M. Nakafuku, and S. Ishii. 1999. Sonic Hedgehog-induced activation of the Gli1 promoter is mediated by GLI3. J. Biol. Chem. 274:8143–8152.
10. Diez del Corral, R., and K. G. Storey. 2004. Opposing FGF and retinoid pathways: a signalling switch that controls differentiation and patterning onset in the extending vertebrate body axis. Bioessays 26:857–869.
11. Di Stefano, V., G. Blandino, A. Sacchi, S. Soddu, and G. D'Orazi. 2004. HIPK2 neutralizes MDM2 inhibition rescuing p53 transcriptional activity and apoptotic function. Oncogene 23:5185–5192.
12. Di Stefano, V., C. Rinaldo, A. Sacchi, S. Soddu, and G. D'Orazi. 2004. Homeodomain-interacting protein kinase-2 activity and p53 phosphorylation are critical events for cisplatin-mediated apoptosis. Exp. Cell Res. 293:311–320.
13. Di Stefano, V., S. Soddu, A. Sacchi, and G. D'Orazi. 2005. HIPK2 contributes to PCAF-mediated p53 acetylation and selective transactivation of p21(Waf1) after nonapoptotic DNA damage. Oncogene 24:5431–5442.
14. D'Orazi, G., B. Cecchinelli, T. Bruno, I. Manni, Y. Higashimoto, S. Saito, M. Gostissa, S. Coen, A. Marchetti, G. Del Sal, G. Piaggio, M. Fanciulli, E. Appella, and S. Soddu. 2002. Homeodomain-interacting protein kinase-2 phosphorylates p53 at Ser 46 and mediates apoptosis. Nat. Cell Biol. 4:11–19.
15. Doxakis, E., E. J. Huang, and A. M. Davies. 2004. Homeodomain-interacting protein kinase-2 regulates apoptosis in developing sensory and sympathetic neurons. Curr. Biol. 14:1761–1765.
16. Ecsedy, J. A., J. S. Michaelson, and P. Leder. 2003. Homeodomain-interacting protein kinase 1 modulates Daxx localization, phosphorylation, and transcriptional activity. Mol. Cell. Biol. 23:950–960.
17. Eggenschwiler, J. T., E. Espinoza, and K. V. Anderson. 2001. Rab23 is an essential negative regulator of the mouse Sonic hedgehog signalling pathway. Nature 412:194–198.
18. el-Deiry, W. S., T. Tokino, V. E. Velculescu, D. B. Levy, R. Parsons, J. M. Trent, D. Lin, W. E. Mercer, K. W. Kinzler, and B. Vogelstein. 1993. WAF1, a potential mediator of p53 tumor suppression. Cell 75:817–825.
19. Engelhardt, O. G., C. Boutell, A. Orr, E. Ullrich, O. Haller, and R. D. Everett. 2003. The homeodomain-interacting kinase PKM (HIPK-2) modifies ND10 through both its kinase domain and a SUMO-1 interaction motif and alters the posttranslational modification of PML. Exp. Cell Res. 283:36–50.
20. Epstein, D. J., M. Vekemans, and P. Gros. 1991. Splotch (Sp2H), a mutation affecting development of the mouse neural tube, shows a deletion within the paired homeodomain of Pax-3. Cell 67:767–774.
21. Fan, C. M., and M. Tessier-Lavigne. 1994. Patterning of mammalian somites by surface ectoderm and notochord: evidence for sclerotome induction by a hedgehog homolog. Cell 79:1175–1186.
22. Fan, C. M., J. A. Porter, C. Chiang, D. T. Chang, P. A. Beachy, and M. Tessier-Lavigne. 1995. Long-range sclerotome induction by sonic hedgehog: direct role of the amino-terminal cleavage product and modulation by the cyclic AMP signaling pathway. Cell 81:457–465.
23. Furumoto, T. A., N. Miura, T. Akasaka, Y. Mizutani-Koseki, H. Sudo, K. Fukuda, M. Maekawa, S. Yuasa, Y. Fu, H. Moriya, M. Taniguchi, K. Imai, E. Dahl, R. Balling, M. Pavlova, A. Gossler, and H. Koseki. 1999. Notochord-dependent expression of MFH1 and PAX1 cooperates to maintain the proliferation of sclerotome cells during the vertebral column development. Dev. Biol. 210:15–29.
24. Gondo, Y., K. Nakamura, K. Nakao, T. Sasaoka, K. Ito, M. Kimura, and M. Katsuki. 1994. Gene replacement of the p53 gene with the lacZ gene in mouse embryonic stem cells and mice by using two steps of homologous recombination. Biochem. Biophys. Res. Commun. 202:830–837.
25. Gresko, E., A. Moller, A. Roscic, and M. L. Schmitz. 2005. Covalent modification of human homeodomain interacting protein kinase 2 by SUMO-1 at lysine 25 affects its stability. Biochem. Biophys. Res. Commun. 329:1293–1299.
26. Harada, J., K. Kokura, C. Kanei-Ishii, T. Nomura, M. M. Khan, Y. Kim, and S. Ishii. 2003. Requirement of the co-repressor homeodomain-interacting protein kinase 2 for ski-mediated inhibition of bone morphogenetic protein-induced transcriptional activation. J. Biol. Chem. 278:38998–39005.
27. Harvey, M., A. T. Sands, R. S. Weiss, M. E. Hegi, R. W. Wiseman, P. Pantazis, B. C. Giovanella, M. A. Tainsky, A. Bradley, and L. A. Donehower. 1993. In vitro growth characteristics of embryo fibroblasts isolated from p53-deficient mice. Oncogene 8:2457–2467.

28. Helwig, U., K. Imai, W. Schmahl, B. E. Thomas, D. S. Varnum, J. H. Nadeau, and R. Balling. 1995. Interaction between undulated and Patch leads to an extreme form of spina bifida in double-mutant mice. Nat. Genet. 11:60–63.
29. Herrera, E., E. Samper, and M. A. Blasco. 1999. Telomere shortening in mTR−/− embryos is associated with failure to close the neural tube. EMBO J. 18:1172–1181.
30. Hofmann, T. G., A. Moller, H. Sirma, H. Zentgraf, Y. Taya, W. Droge, H. Will, and M. L. Schmitz. 2002. Regulation of p53 activity by its interaction with homeodomain-interacting protein kinase-2. Nat. Cell Biol. 4:1–10.
31. Hofmann, T. G., N. Stollberg, M. L. Schmitz, and H. Will. 2003. HIPK2 regulates transforming growth factor-β-induced c-Jun NH_2-terminal kinase activation and apoptosis in human hepatoma cells. Cancer Res. 63:8271–8277.
32. Hofmann, T. G., E. Jaffray, N. Stollberg, R. T. Hay, and H. Will. 2005. Regulation of homeodomain-interacting protein kinase 2 (HIPK2) effector function through dynamic SUMO-1 modification. J. Biol. Chem. 280:29224–29232.
33. Hogan, B., R. Beddington, F. Costantini, and E. Lacy. 1994. Isolation, culture, and manipulation of embryonic stem cells, p. 253–290. *In* B. Hogan, F. Costantini, and E. Lacy (ed.), Manipulating the mouse embryo: a laboratory manual, 2nd ed. Cold Spring Harbor Laboratory Press, Cold Spring Harbor, N.Y.
34. Hollander, M. C., M. S. Sheikh, D. V. Bulavin, K. Lundgren, L. Augeri-Henmueller, R. Shehee, T. A. Molinaro, K. E. Kim, E. Tolosa, J. D. Ashwell, M. P. Rosenberg, Q. Zhan, P. M. Fernandez-Salguero, W. F. Morgan, C. X. Deng, and A. J. Fornace, Jr. 1999. Genomic instability in Gadd45a-deficient mice. Nat. Genet. 23:176–184.
35. Juriloff, D. M., and M. J. Harris. 2000. Mouse models for neural tube closure defects. Hum. Mol. Genet. 9:993–1000.
36. Kanei-Ishii, C., J. Ninomiya-Tsuji, J. Tanikawa, T. Nomura, T. Ishitani, S. Kishida, K. Kokura, T. Kurahashi, E. Ichikawa-Iwata, Y. Kim, K. Matsumoto, and S. Ishii. 2004. Wnt-1 signal induces phosphorylation and degradation of c-Myb protein via TAK1, HIPK2, and NLK. Genes Dev. 18:816–829.
37. Kim, Y. H., C. Y. Choi, S. J. Lee, M. A. Conti, and Y. Kim. 1998. Homeodomain-interacting protein kinases, a novel family of co-repressors for homeodomain transcription factors. J. Biol. Chem. 273:25875–25879.
38. Kim, Y. H., C. Y. Choi, and Y. Kim. 1999. Covalent modification of the homeodomain-interacting protein kinase 2 (HIPK2) by the ubiquitin-like protein SUMO-1. Proc. Natl. Acad. Sci. USA 96:12350–12355.
39. Kondo, S., Y. Lu, M. Debbas, A. W. Lin, I. Sarosi, A. Itie, A. Wakeham, J. Tuan, C. Saris, G. Elliott, W. Ma, S. Benchimol, S. W. Lowe, T. W. Mak, and S. K. Thukral. 2003. Characterization of cells and gene-targeted mice deficient for the p53-binding kinase homeodomain-interacting protein kinase 1 (HIPK1). Proc. Natl. Acad. Sci. USA 100:5431–5436.
40. Li, X., R. Zhang, D. Luo, S. J. Park, Q. Wang, Y. Kim, and W. Min. 2005. Tumor necrosis factor alpha-induced desumoylation and cytoplasmic translocation of homeodomain-interacting protein kinase 1 are critical for apoptosis signal-regulating kinase 1-JNK/p38 activation. J. Biol. Chem. 280:15061–15070.
41. Lohnes, D. 2003. The Cdx1 homeodomain protein: an integrator of posterior signaling in the mouse. Bioessays 25:971–980.
42. McMahon, J. A., S. Takada, L. B. Zimmerman, C. M. Fan, R. M. Harland, and A. P. McMahon. 1998. Noggin-mediated antagonism of BMP signaling is required for growth and patterning of the neural tube and somite. Genes Dev. 12:1438–1452.
43. Miyashita, T., and J. C. Reed. 1995. Tumor suppressor p53 is a direct transcriptional activator of the human bax gene. Cell 80:293–299.
44. Moilanen, A. M., U. Karvonen, H. Poukka, O. A. Janne, and J. J. Palvimo. 1998. Activation of androgen receptor function by a novel nuclear protein kinase. Mol. Biol. Cell 9:2527–2543.
45. Moller, A., H. Sirma, T. G. Hofmann, S. Rueffer, E. Klimczak, W. Droge, H. Will, and M. L. Schmitz. 2003. PML is required for homeodomain-interacting protein kinase 2 (HIPK2)-mediated p53 phosphorylation and cell cycle arrest but is dispensable for the formation of HIPK domains. Cancer Res. 63:4310–4314.
46. Moller, A., H. Sirma, T. G. Hofmann, H. Staege, E. Gresko, K. S. Ludi, E. Klimczak, W. Droge, H. Will, and M. L. Schmitz. 2003. Sp100 is important for the stimulatory effect of homeodomain-interacting protein kinase-2 on p53-dependent gene expression. Oncogene 22:8731–8737.
47. Oda, K., H. Arakawa, T. Tanaka, K. Matsuda, C. Tanikawa, T. Mori, H. Nishimori, K. Tamai, T. Tokino, Y. Nakamura, and Y. Taya. 2000. p53AIP1, a potential mediator of p53-dependent apoptosis, and its regulation by Ser-46-phosphorylated p53. Cell 102:849–862.
48. Packer, A. I., D. A. Crotty, V. A. Elwell, and D. J. Wolgemuth. 1998. Expression of the murine Hoxa4 gene requires both autoregulation and a conserved retinoic acid response element. Development 125:1991–1998.
49. Pani, L., M. Horal, and M. R. Loeken. 2002. Rescue of neural tube defects in Pax-3-deficient embryos by p53 loss of function: implications for Pax-3-dependent development and tumorigenesis. Genes Dev. 16:676–680.
50. Peters, H., B. Wilm, N. Sakai, K. Imai, R. Maas, and R. Balling. 1999. Pax1 and Pax9 synergistically regulate vertebral column development. Development 126:5399–5408.
51. Pierantoni, G. M., M. Fedele, F. Pentimalli, G. Benvenuto, R. Pero, G. Viglietto, M. Santoro, L. Chiariotti, and A. Fusco. 2001. High mobility group I (Y) proteins bind HIPK2, a serine-threonine kinase protein which inhibits cell growth. Oncogene 20:6132–6141.
52. Pierantoni, G. M., A. Bulfone, F. Pentimalli, M. Fedele, R. Iuliano, M. Santoro, L. Chiariotti, A. Ballabio, and A. Fusco. 2002. The homeodomain-interacting protein kinase 2 gene is expressed late in embryogenesis and preferentially in retina, muscle, and neural tissues. Biochem. Biophys. Res. Commun. 290:942–947.
53. Puri, P. L., K. Bhakta, L. D. Wood, A. Costanzo, J. Zhu, and J. Y. Wang. 2002. A myogenic differentiation checkpoint activated by genotoxic stress. Nat. Genet. 32:585–593.
54. Rastegar, M., L. Kobrossy, E. N. Kovacs, I. Rambaldi, and M. Featherstone. 2004. Sequential histone modifications at Hoxd4 regulatory regions distinguish anterior from posterior embryonic compartments. Mol. Cell. Biol. 24:8090–8103.
55. Rochat-Steiner, V., K. Becker, O. Micheau, P. Schneider, K. Burns, and J. Tschopp. 2000. FIST/HIPK3: a Fas/FADD-interacting serine/threonine kinase that induces FADD phosphorylation and inhibits Fas-mediated Jun NH_2-terminal kinase activation. J. Exp. Med. 192:1165–1174.
56. Roelink, H., J. A. Porter, C. Chiang, Y. Tanabe, D. T. Chang, P. A. Beachy, and T. M. Jessell. 1995. Floor plate and motor neuron induction by different concentrations of the amino-terminal cleavage product of Sonic hedgehog autoproteolysis. Cell 81:445–455.
57. Rui, Y., Z. Xu, S. Lin, Q. Li, H. Rui, W. Luo, H. M. Zhou, P. Y. Cheung, Z. Wu, Z. Ye, P. Li, J. Han, and S. C. Lin. 2004. Axin stimulates p53 functions by activation of HIPK2 kinase through multimeric complex formation. EMBO J. 23:4583–4594.
58. Saga, Y., N. Hata, H. Koseki, and M. M. Taketo. 1997. Mesp2: a novel mouse gene expressed in the presegmented mesoderm and essential for segmentation initiation. Genes Dev. 11:1827–1839.
59. Sah, V. P., L. D. Attardi, G. J. Mulligan, B. O. Williams, R. T. Bronson, and T. Jacks. 1995. A subset of p53-deficient embryos exhibit exencephaly. Nat. Genet. 10:175–180.
60. Sung, K. S., Y. Y. Go, J. H. Ahn, Y. H. Kim, Y. Kim, and C. Y. Choi. 2005. Differential interactions of the homeodomain-interacting protein kinase 2 (HIPK2) by phosphorylation-dependent sumoylation. FEBS Lett. 579:3001–3008.
61. Takebayashi-Suzuki, K., J. Funami, D. Tokumori, A. Saito, T. Watabe, K. Miyazono, A. Kanda, and A. Suzuki. 2003. Interplay between the tumor suppressor p53 and TGF beta signaling shapes embryonic body axes in Xenopus. Development 130:3929–3939.
62. Wallin, J. W., H. Koseki, R. Fritsch, B. Christ, and R. Balling. 1994. The role of *Pax1* in axial skeleton development. Development 120:1109–1121.
63. Wang, Y., E. M. Schneider, X. Li, I. Duttenhofer, K. Debatin, and H. Hug. 2002. HIPK2 associates with RanBPM. Biochem. Biophys. Res. Commun. 297:148–153.
64. Watanabe, K., T. Ozaki, T. Nakagawa, K. Miyazaki, M. Takahashi, M. Hosoda, S. Hayashi, S. Todo, and A. Nakagawara. 2002. Physical interaction of p73 with c-Myc and MM1, a c-Myc-binding protein, and modulation of the p73 function. J. Biol. Chem. 277:15113–15123.
65. Wiggins, A. K., G. Wei, E. Doxakis, C. Wong, A. A. Tang, K. Zang, E. J. Luo, R. L. Neve, L. F. Reichardt, and E. J. Huang. 2004. Interaction of Brn3a and HIPK2 mediates transcriptional repression of sensory neuron survival. J. Cell Biol. 167:257–267.
66. Ybot-Gonzalez, P., P. Cogram, D. Gerrelli, and A. J. Copp. 2002. Sonic hedgehog and the molecular regulation of mouse neural tube closure. Development 129:2507–2517.
67. Zakany, J., M. Kmita, P. Alarcon, J. L. de la Pompa, and D. Duboule. 2001. Localized and transient transcription of Hox genes suggests a link between patterning and the segmentation clock. Cell 106:207–217.
68. Zhang, Q., Y. Yoshimatsu, J. Hildebrand, S. M. Frisch, and R. H. Goodman. 2003. Homeodomain interacting protein kinase 2 promotes apoptosis by downregulating the transcriptional corepressor CtBP. Cell 115:177–186.
69. Zhang, Q., A. Nottke, and R. H. Goodman. 2005. Homeodomain-interacting protein kinase-2 mediates CtBP phosphorylation and degradation in UV-triggered apoptosis. Proc. Natl. Acad. Sci. USA 102:2802–2807.

Oncogene (2006) 25, 1931–1942

www.nature.com/onc

ORIGINAL ARTICLE

Increased expression of proapoptotic *BMCC1*, a novel gene with the *BNIP2* and *Cdc42GAP* homology (BCH) domain, is associated with favorable prognosis in human neuroblastomas

T Machida[1,2,5], T Fujita[1,2,5], ML Ooo[1], M Ohira[1], E Isogai[1], M Mihara[1,2], J Hirato[3], D Tomotsune[1], T Hirata[4], M Fujimori[2], W Adachi[2] and A Nakagawara[1]

[1]*Division of Biochemistry, Chiba Cancer Center Research Institute, Chiba, Japan;* [2]*Department of Surgery, Shinshu University School of Medicine, Matsumoto, Nagano, Japan;* [3]*Department of Pathology, Gunma University School of Medicine, Maebashi, Gunma, Japan and* [4]*Hisamitsu Pharmaceutical Co., Inc., Tokyo, Japan*

Differential screening of the genes obtained from cDNA libraries of primary neuroblastomas (NBLs) between the favorable and unfavorable subsets has identified a novel gene *B*CH *m*otif-containing molecule at the *c*arboxyl terminal region *1* (*BMCC1*). Its 350 kDa protein product possessed a Bcl2-/adenovirus E1B nineteen kDa-interacting protein 2 (BNIP2) and Cdc42GAP homology domain in the COOH-terminus in addition to P-loop and a coiled-coil region near the NH_2-terminus. High levels of *BMCC1* expression were detected in the human nervous system as well as spinal cord, brain and dorsal root ganglion in mouse embryo. The immunohistochemical study revealed that BMCC1 was positively stained in the cytoplasm of favorable NBL cells but not in unfavorable ones with *MYCN* amplification. The quantitative real-time reverse transcription–PCR using 98 primary NBLs showed that high expression of *BMCC1* was a significant indicator of favorable NBL. In primary culture of newborn mice superior cervical ganglion (SCG) neurons, m*BMCC1* expression was downregulated after nerve growth factor (NGF)-induced differentiation, and upregulated during the NGF-depletion-induced apoptosis. Furthermore, the proapoptotic function of BMCC1 was also suggested by increased expression in CHP134 NBL cells undergoing apoptosis after treatment with retinoic acid, and by an enhanced apoptosis after depletion of NGF in the SCG neurons obtained from newborn mice transgenic with *BMCC1* in primary culture. Thus, BMCC1 is a new member of prognostic factors for NBL and may play an important role in regulating differentiation, survival and aggressiveness of the tumor cells.
Oncogene (2006) **25**, 1931–1942. doi:10.1038/sj.onc.1209225; published online 14 November 2005

Keywords: BMCC1; neuroblastoma; apoptosis; BNIP2; Cdc42GAP; BCH domain

Correspondence: Dr A Nakagawara, Division of Biochemistry, Chiba Cancer Center Research Institute, 666-2 Nitona, Chuoh-ku, Chiba 260-8717, Japan.
E-mail: akiranak@chiba-cc.jp
[5]These authors contributed equally to this work.
Received 13 April 2005; revised 15 September 2005; accepted 29 September 2005; published online 14 November 2005

Introduction

Neuroblastoma (NBL) is one of the most common pediatric neoplasms and originates from the sympathoadrenal lineage of neural crest. However, its biological as well as clinical behavior is highly heterogeneous. The tumors occurred in the patients under 1 year of age have a tendency to spontaneously regress or differentiate (Evans *et al.*, 1976). On the other hand, the tumors found in the patients more than 1 year of age are usually aggressive and often kill the patients. The latter subsets of the tumor frequently have multiple genomic aberrations which include frequent loss of the distal part of the short arm of chromosome 1, amplification of the *MYCN* oncogene, and gain of chromosome 17q, all of which are associated with unfavorable prognosis (Brodeur *et al.*, 1984; Caron, 1995).

Although the molecular mechanism underlying regression of NBL is still unclear, accumulating evidence suggests that the signals from neurotrophic factors and their receptors play an important role in regulating growth, differentiation and programmed cell death. High expression of *TrkA*, a high affinity receptor for nerve growth factor (NGF), is associated with the favorable outcome, and there is an inverse correlation between *TrkA* expression and *MYCN* amplification. Cells expressing functional TrkA may be susceptible to either programmed cell death leading to tumor regression, especially in infants, or to differentiation to a benign ganglioneuroma. Thus, like normal sympathetic neurons, a limited amount of NGF may be supplied from the stromal cells such as Schwann cells and fibroblasts, that at least partly regulates differentiation and programmed cell death of the NBL cells. In contrast, TrkB, another family member, is preferentially expressed in aggressive NBL cells together with its preferred ligands BDNF and NT-4/5 which stimulate proliferation in an autocrine/paracrine manner, conferring potency to invade and/or metastasize on the tumor cells (Nakagawara *et al.*, 1993, 1994).

The proto-oncogene *bcl-2* encodes a 25-kDa mitochondrial membrane protein that inhibits programmed cell death (Hockenbery *et al.*, 1990; Garcia *et al.*, 1992;

Oltvai *et al*., 1993). The recent reports have suggested that *bcl-2* protein is expressed at relatively high levels in both NBLs and neural crest cells. However, the role of *bcl-2* in the regulation of differentiation and survival of NBL cells is still elusive.

In order to clarify the molecular mechanism of cellular signaling related to regression of NBL, we have cloned a large number of genes from full-length-enriched oligo-capping cDNA libraries constructed from two different subsets of NBL with favorable and unfavorable biology (Ohira *et al*., 2003a, b). Sequence analysis of the genes from those libraries has revealed that the expression profile is significantly different between the both subsets. Screening by using semiquantitative RT–PCR has shown that more than 500 genes are differentially expressed between them. In the present paper, we report cloning and functional characterization of a novel gene termed as *B*cl2-/adenovirus E1B *n*ineteen kDa-*i*nteracting *p*rotein *2* (*B*NIP2) and *Cdc42GAP* homology *B*CH *m*otif-containing molecule at the *c*arboxyl terminal region *1* (*BMCC1*), which is preferably expressed in favorable NBL.

Results

Full-length cDNA cloning and structural analysis of the BMCC1 *gene*

As reported previously, we constructed oligo-capping cDNA libraries from different subsets of primary NBLs (Ohira *et al*., 2003b). After DNA sequencing both ends of about 10 000 clones randomly picked up, we obtained 5000 independent genes, among which about 2000 were found to be novel by homology search. They were then subjected to semi-quantitative RT–PCR to examine if they are differentially expressed between favorable (stage 1, less than 1-year-old, single copy of *MYCN* and high expression of *TrkA*) and unfavorable (stage 3 or 4, more than 1-year-old, amplified *MYCN* and low expression of *TrkA*) subsets of NBL. The differential screening in a panel of template cDNAs obtained from 16 favorable and 16 unfavorable primary NBLs demonstrated an interesting novel gene (*Nbla00219*) which had a BNIP2 and BCH domain, a recently reported new motif which might interact with Bcl-2 protein, at the COOH-terminus. It was preferentially expressed in favorable NBLs.

Sequencing of the *Nbla00219* clone showed that the insert size was 2277 bp with a putative open reading frame (ORF) of 1452 bp (484 amino acids) localized at the 5′-end region. The database search demonstrated that the *Nbla00219* sequence matched to the *KIAA0367* cDNA (accession no.: AB002365) with 95% identity as well as a part of the genomic sequence within the BAC clone RP11-146P9 (GenBank accession no.: AL161625) which was mapped to chromosome 9p13. However, there was no in-frame stop codon in the upstream region of the putative initiation site of *KIAA0367*, suggesting that the coding region of the gene extended over the 5′-end. In fact, Northern blot analysis of human fetal brain mRNA using *nbla00219* cDNA as a probe demonstrated that the transcript size was approximately 12 kb (Figure 1d). In order to determine a full-length cDNA of this gene, we performed gene prediction according to the sequence information from the BAC clone RP11-146P9 by using several algorithm. The exons expected in the upstream region of the gene were confirmed by RT–PCR using cDNA libraries constructed from human fetal brain and/or NBL tissues with favorable prognosis as template with subsequent DNA sequencing. It revealed that the gene contained a large exon of about 6.5 kb within the extended 5′-coding region. The predicted 5′-side ORF was also confirmed by matching to the several mouse ESTs. Then, we finally identified the full-length *Nbla00219* cDNA (Figure 1a) with a 5′-untranslated region of 323 bp (nt. no. 1-323), an ORF of 8355 bp (nt. no. 324-8497), and a 3′-untranslated region of 3196 bp (nt. no. 8498-11 690) (accession no.: AB050197). The Kozak consensus sequence for translation initiation site (Kozak, 1987) was found at the putative ATG start codon (at position 324), though no in-frame stop codon was found in the upstream region. The blast search against public databases showed no significant homology except BNIP2 (accession no.: XM007602, 52% identity) and Cdc42GAP (accession no.: NM004308, 38% identity) at the COOH-terminal end of the full-length *Nbla00219* (Figure 1a and b). Since the region had been termed as the BCH domain which was highly conserved among the three genes (Figure 1c), we named the full-length *Nbla00219* gene as *BMCC1*.

The BCH domain acts as the GTPase activating protein (GAP) in BNIP2. There are two critical arginine residues, Arg-236 and Arg-238, which are important for conferring the GAP activity to the Cdc42 homodimers (Zhang and Zheng, 1998; Zhang *et al*., 1999; Low *et al*., 2000). In BMCC1, both critical arginine residues were well conserved. Using several algorithms to predict the secondary structure of amino acids and the intracellular localization, we found the coiled-coil motif (amino acids 918–941) and P-loop (amino acids 2293–2300) within the BMCC1 protein (Figure 1a). Three putative transmembrane domains (amino acids 2545–2563, 2573–2597 and 2632–2653) were also suggested.

Although *BMCC1* was expressed significantly at higher levels in favorable than unfavorable NBLs, the expression levels of *BNIP2 family* were similar between the NBL subsets (Figure 2a).

Expression of BMCC1 *in human tissues and cell lines*

To study the expression pattern of *BMCC1* mRNA in human tissues, we performed semiquantitative RT–PCR. *BMCC1* was expressed in many tissues examined except for bone marrow, thymus and spleen (Figure 2c). The high levels of expression were seen in the nervous system (brain, cerebellum and spinal cord) as well as adrenal gland which were the tissues NBL originated from. We further performed semiquantitative RT–PCR to examine the expression levels of *BMCC1* in cultured cell lines including NBL and other cancers. *BMCC1* was expressed in most of 17 NBL cell lines tested (Figure 2b). Among the other cancer lines, high expression of *BMCC1* was observed in rhabdomyosar-

a

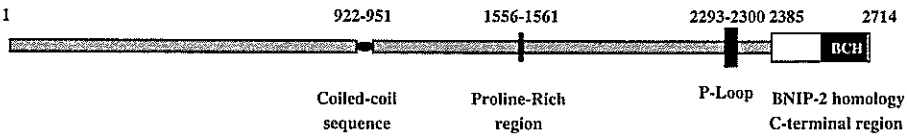

b

```
MVSNSRTSSTEAVAGSAPLSQGSSGIMELYGSDIEPQPSSVNFIENPPDLNDSNQAQVDANVDLVSPDSGLATIRSSRSSKESSVFLSDDSPVGEGAGPH 100
HTLLPGLDSYSPIPEGAVAEEHAWSGEHGEHFDLFNFDPAPMASGQSQQSSHSADYSPADDFFPNSDLSEGQLPAGPEGLDGMGTNMSNYSSSSLLSGAG 200
KDSLVEHDEEFVQRQDSPRDNSERNLSLTDFVGDESPSPERLKNTGKRIPPTPMNSLVESSPSTEEPASLYTEDTTQKATDTGHMGPPQTHARRSSWWGG 300
LEIDSKNIADAWSSSEQESVFQSPESWKEHKPSSIDRRASDSVFQPKSLEFTKSGPWESEFGQPELGSNDIQDKNEESLPFQNLPMEKSPLPNTSPQGTN 400
HLIEDFASLWHSGRSPTAMPEPWGNPTDDGEPAAVAPFPAWSAFGKEDHDEALKNTWDLHPTSSKTPSVRDPNEWAMAKSGFAFSSSELLDNSPSEINNE 500
AAPEIWGKKNNDSRDHIFAPGNPSSDLDHTWTNSKPPKEDQNGLVDPKTRGKVYEKVDSWNLFEENMKKGGSDVLVPWEDSFLSYKCSDYSASNLGEDSV 600
PSPLDTNYSTSDSYTSPTFAGDEKETEHKPFAKEEGFESKDGNSMAEETDIPPQSLQQSLQQSSRNRISSGPGNLDMWASPHTDNSSEINTTHNLDENEL 700
KTEHTDGKNISMEDDVGESSQSSYDDPSMMQLYNETNRQLTLLHSSTNSRQTAPDSLDLWNRVILEDTQSTATISDMDNDLDWDDCSGGAAIPSDGQTEG 800
YMAEGSEPETRFTVRQLEPWGLEYQEANQVDWELPASDEHTKDSAPSEHHTLNEKSGQLIANSIWDSVMRDKDMSSFMLPGSSHITDSEQRELPPEIPSH 900
SANVKDTHSPDAPAASGTSESEALISHLDKQDTERETLQSDAASLATRLENPGYFPHPDPRKGHGDGQSESEKEAQGATDRGHLDEEEVIASGVENASGI 1000
SEKGQSDQELSSLVASEHQEICIKSGKISSLAVTFSPQTEEPEEVLEYEEGSYNLDSRDVQTGMSADNLQPKDTHEKHLMSQRNSGETTETSDGMNFTKY 1100
VSVPEKDLEKTEECNFLEPENVGGGPPHRVPRSLDFGDVPIDSDVHVSNTRSEITKNLDVKGSENSLPGAGSSGNFDRDTISSEYTHSSASSPELNDSSV 1200
ALSSWGQQPSSGYQEENQGNWSEQNHQESELITTDGQVEIVTKVKDLEKNRINEFEKSFDRKTPTFLEIWNDSVDGDSFSSLSSPETGKYSEHSGTHQES 1300
NLIASYQEKNEHDISATVQPEDARVISTSSGSDDDSVGGEESIEEEIQVANCNVAEDESRAWDSLNESNEFLVTADPKSENIYDYLDSSEPAENENKSNP 1400
FCDNQQSSPDPWTFSPLTETEMQITAVEKEKRSSPETGTTGDVAWQISPKASFPKNEDNSQLEMLGFSADSTEWWTSPQEGRLIESPFERELSDSSGVLE 1500
INSSVHQNASPWGVPVQGDIEPVETHYTNPFSDNHQSPFLEGNGKNSHEQLWNIQPRQPDPDADKFSQLVKLDQIKEKDSREQTFVSAAGDELTPETPTQ 1600
EQCQDTMLPVCDHPDAAFTHAEENSCVTSNVSTNEGQETNQWEQEKSYLGEMTNSSIATENFPAVSSPTQLIMKPGSEWDGSTPSEDSRGTFVPDILHGN 1700
FQEGGQLASAAPDLWMDAKKPFSLKADGENPDILTHCEHDSNSQASDSPDICHDSEAREETEKHLSACMGPEVESSELCLTEPEIDEEPIYEPGREFVPS 1800
NAELDSENATVLPPIGYQADIKGSSQPTSHKGSPEPSEINGDNSTGLQVSEKGASPDMAPILEPVDRRIPRIENVATSIFVTHQEPTPEGDGSWISDSFS 1900
PESQPGARALFDGDPHLSTENPALVPDALLASDTCLDISEAAFDHSFSDASGLNTSTGTIDDMSKLTLSEGHPETPVDGDLGKQDICSSEASWGDFEYDV 2000
MGQNIDEDFLREPEHFLYGGDPPLEEDSLKQSLAPYTPPFDLSYLTEPAQSAETIEEAGSPEDESLGCRAAEIVLSALPDRRSEGNQAETKNRLPGSQLA 2100
VLHIREDPESVYLPVGAGSNILSPSNVDWEVETDNSDLPAGGDIGPPNGASKEIPELEEEKTIPTKEPEQIKSEYKEERCTEKNEDRHALHMDYILVNRE 2200
ENSHSKPETCEERESIAELELYVGSKETGLQGTQLASFPDTCQPASLNERKGLSAEKMSSKGDTRSSFESPAQDQSWMFLGHSEVGDPSLDARDSGPGWS 2300
GKTVEPFSELGLGEGPQPQILEEMKPLESLALEEASGPVSQSQKSKSRGRAGPDAVTHDNEWEMLSPQPVQKTMIPDTEMEEETEFLELGTRISRPNGLL 2400
SEDVGMDIPFEEGVLSPSAADMRPEPPNSLDLNDTHPRRIKLTAPNINLSLDQSEGSILSDDNLDSPDEIDINVDELDTPDEADSFEYTGHDPTANKDSG 2500
QESESIPEYTAEEEREDNRLWRTVVIGEQEQRIDMKVIEPYRRVISHGGYYGDGLNAITVFAACFLPDSSRADYHYVMENLFLYVISTLELMVAEDYMIV 2600
YLNGATPRRRMPGLGWMKKCYQMIDRRLRKNLKSFIIVHPSWFIRTILAVTRPFISSKFSSKIKYVNSLPELSGLIPMDCIHIPESIIKTSCLYNDPEMS 2700
SMEKDIDLKLKEKP 2714
```

c

```
BMCC1       2542:RRVISHGG------YYGDGLNAIIVFAACFLPDSSRADYHYVMENLFLYVISTLE LMVAEDYMIVYLNGATPRRRMPGLGWMKKCYQMI
BNIP2        151:KKVISHGG------YYGDGLNAIVVFAVCFMPESSQPNYRYLMDNLFKYVIGTLE LLVAENYMIVYLNGATTRRKMPSLGWLRKCYQQI
BNIP-Salpha  117:KKVLSHGG------YHGDGLNAVILFASCYLPRSSIPNYTYVMEHLFRYMVGTLE LLVAENYLLVHLSGGTSRAQVPPLSWIRQCYRTL
BNIP-Sbeta   117:KKVLSHGG------YHGDGLNAVILFASCYLPRSSIPNYTYVMEHLFRYMVGTLE LLVAENYLLVHLSGGTSRAQVPPLSWIRQCYRTL
Cdc42GAP      85:----------------------IIVFSACRMPPSHQLDHSKLLG----YLKHTLD QYVESDYTLLYLHHGLTSDNKPSLSWLRDAYREF

BMCC1       2646:DRRLRKNLKSFIIVHPSWFIRTILAVTRPFISSKFSSKIKYVNSLPELSGLIPMDCIHIPESIIKTSCLYNDPEMS SMEKDIDLKLKEKP 2714 (100%)
BNIP2        234:DRRLRKNLKSLIIVHPSWFIRTLLAVTRPFISSKFSQKIRYVFNLAELAELVPMEYVGIPECI-KQVDQELNG-KQ DEPKNEQ------- 314 (57%)
BNIP-Salpha  200:DRRLRKNLRALVVVHATWYVKAFLALLRPFISSKFTRKIRFLDSLGELAQLISLDQVHIPEAVRQLDRDLHGSGGT -------------- 275 (41%)
BNIP-Sbeta   200:DRRVL---------------------------------------------------------------------- -------------- 204 (42%)
Cdc42GAP     148:DRKYKKNIKALYIVHPTMFIKTLLILFKPLISFKFGQKIFYVNYLSELSEHVKLEQLGIPRQVLK----YDDFLKS TQKSP--------- 224 (34%)
```

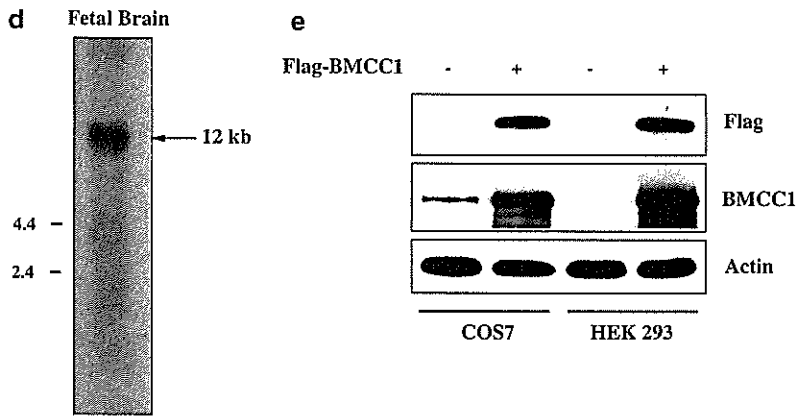

Figure 1 Molecular cloning of BMCC1. (a) Schematic structure of BMCC1. BMCC1 contains coiled-coil sequence, proline-rich region, P-loop and BCH domain in its concurrent position. (b) Full-length amino-acid sequence of human BMCC1. Coiled-coil, proline-rich and P-loop regions were underlined and BCH domain was indicated in box. (c) Alignment of C-terminal regions of BMCC1, BNIP-2, BNIP-Salpha, BNIP-Sbeta, and Cdc42GAP homologous to BCH domain. Total number of amino-acid residues of each protein and their percent homology were described at the end of each sequence. RRKMP (homophilic/heterophilic dimerized sequence), EYV (binding to switch I and insert region of Cdc42) (Low *et al*., 2000) and RRLRK (arginine patch of BCH domain), ATWYVKA (binding motif for homophilic complex and critical for proapoptotic activity) (Zhou *et al*., 2002), were underlined. (d) Northern blot analysis of *BMCC1* transcript in fetal brain tissue. Total RNA (25 μg) purchased from Clontech was loaded for Northern blotting. Left; size markers showing 2.4 and 4.4 kb. (e) BMCC1 expression in COS7 and HEK293 cells. pCAGGS-BMCC1-Flag was transfected into COS7 and HEK 293 cells and lysed after 48 h. Cell lysates were run into 8% SDS–PAGE in 35 mA for more than 4 h, transferred to immobilon-P membrane (MILLIPORE) and probed by anti-Flag, anti-BMCC1 (C-terminal end epitope), and antiactin antibodies.

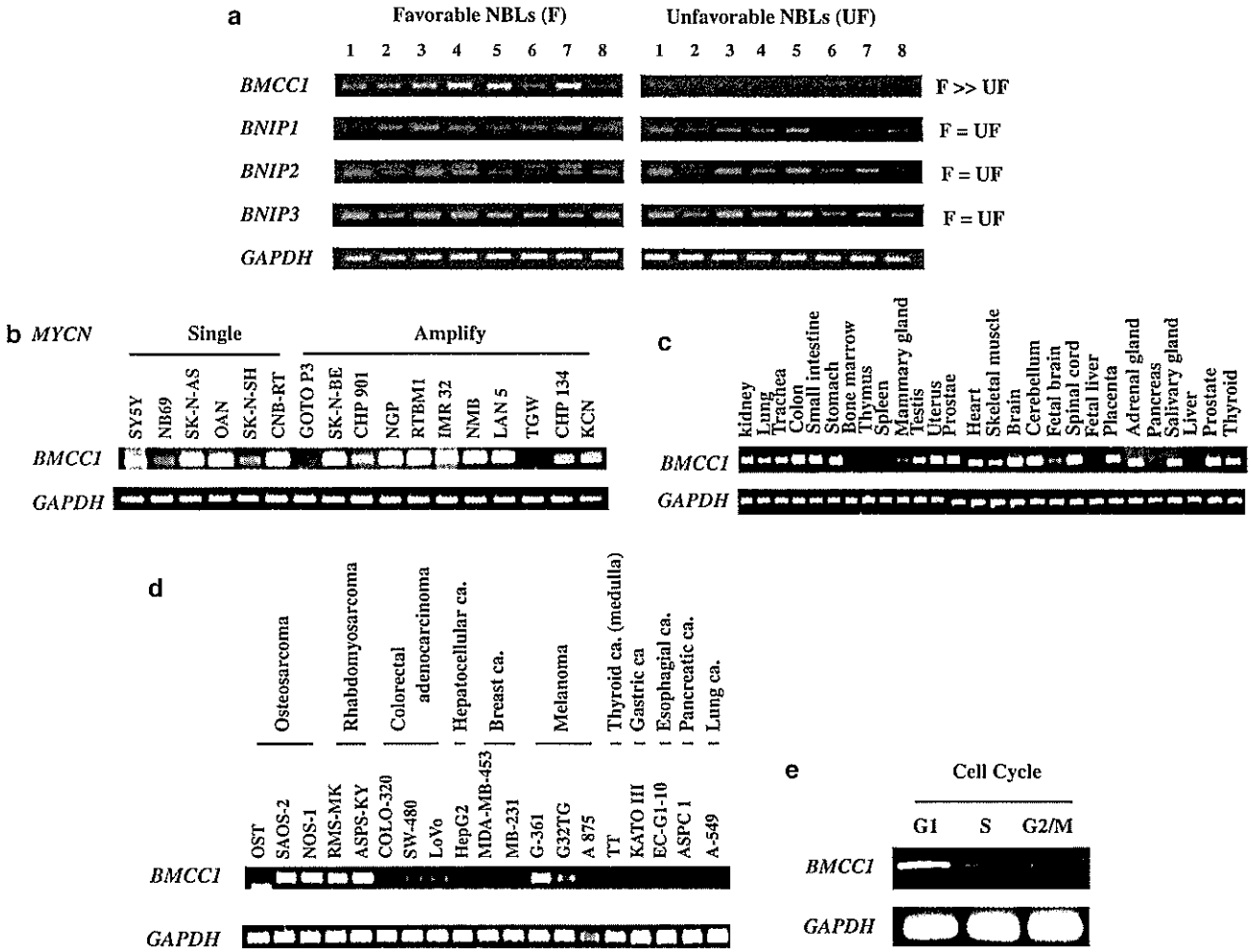

Figure 2 Expression of *BMCC1* mRNA. (a) Differential expression of *BMCC1* in favorable and unfavorable neuroblastomas. mRNA expression patterns for *BMCC1* and *BNIP* gene family members were detected by semiquantitative RT–PCR procedure. Results for eight favorable and eight unfavorable NBLs are shown. The expression of *GAPDH* is also shown as a control. Lanes 1–8: favorable NBLs (F; stage 1 or 2, with a single copy of *MYCN*), lanes 9–6: unfavorable NBLs (UF; stage 3 or 4, with *MYCN* amplification). (b) Expression of *BMCC1* mRNA in neuroblastoma cell lines. In all, 11 NBL cell lines with *MYCN* amplification and six cell lines with a single copy of *MYCN* were used for semiquantitative RT–PCR as templates. (c) Semiquantitative RT–PCR of *BMCC1* in multiple human tissues. Total RNA of 25 adult tissues and two fetal tissues were purchased from Clontech Co. Ltd. As a control, same cDNA templates were amplified by *GAPDH* primers. (d) Expression of *BMCC1* mRNA in the other cancer cell lines. Semiquantitative RT–PCR analysis was performed using cDNA primers and control *GAPDH* primers. Tumor origins were shown on the top. (e) The changes in expression of *BMCC1* at the cell cycle stages. HeLa cells were synchronized by treatment with 400 μM mimosine for 18 h (G1-phase arrest), with 2 mM thymidine for 20 h (S-phase arrest), or with 0.6 μg/ml nocodazole for 18 h (G2/M-phase arrest) and collected for RNA isolation. Semiquantitative RT–PCR was conducted by using *BMCC1* primers and *GAPDH* control primers.

coma, melanoma and some osteosarcoma cell lines, whereas only low levels of expression were found in cancer cell lines of liver, breast, thyroid and colon (Figure 2d). We further examined the cell cycle-dependent expression of *BMCC1* mRNA in HeLa cells by using semiquantitative RT–PCR. As shown in Figure 2e, *BMCC1* was predominantly expressed in G1 phase of the cell cycle.

In situ *hybridization of* BMCC1 *in mouse embryo*

In situ hybridization in mouse embryo showed that *BMCC1* was specifically expressed in neural tube and neural crest-related tissues. In E10.5 mouse embryo, *BMCC1* was highly expressed in neural tube and pharyngeal arches which are derived from neural crest. The expression of *BMCC1* seemed to be more restricted in the later stages of development (Figure 3). In E12.5 mouse embryo (Figure 3d), *BMCC1* was expressed in spinal cord, hindbrain, midbrain, forebrain and dorsal root ganglia (DRG). Although the expressions of *BMCC1* in E14.5 mouse embryos (Figure 3a and b) were similar to those in E12.5, the regions expressing *BMCC1* in hindbrain (Figure 3a), spinal cord and forebrain at E14.5 (Figure 3b) were more dorsally restricted than at E12.5.

Immunohistochemical staining of BMCC1 in primary NBLs

The favorable NBLs occasionally expressed BMCC1 in the cytoplasm of the tumor cells (Figure 4b). In contrast,

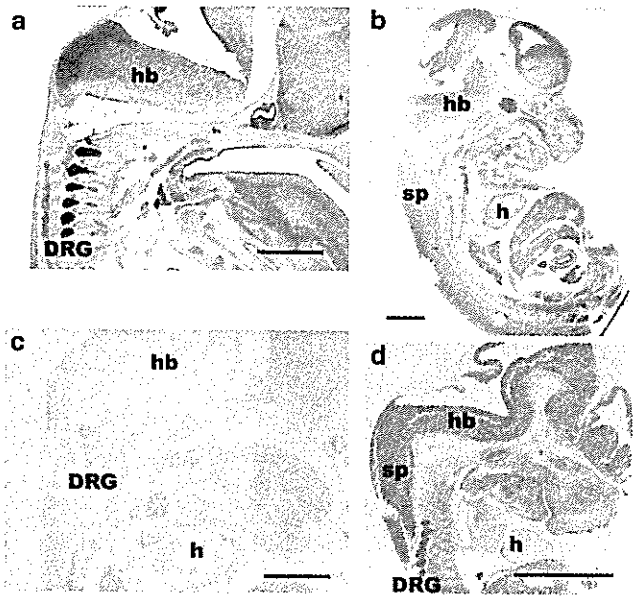

Figure 3 Section *in situ* hybridization of embryos with the *BMCC1* probe. Sagittal sections of embryos at E14.5 (a–c) and E12.5 (d) were prepared and the *BMCC1* expression was examined by section *in situ* hybridization. (a), (b) and (d) Antisense probes. (c) Sense probe (control). The *BMCC1* probe used is described in the Experimental procedures. DRG, dorsal root ganglion; sp, spinal cord; hb, hindbrain; h, heart. Scale bar, 200 μm.

in the unfavorable neuroblastomas the tumor cells were entirely negative for BMCC1 or only a few positive cells were observed (Figure 4d).

Prognostic significance of BMCC1 *mRNA expression in human NBLs*

The levels of *BMCC1* mRNA expression were measured in 98 primary NBLs by using quantitative real-time RT–PCR. The high levels of *BMCC1* expression were significantly associated with favorable NBL in stages 1, 2 and 4 (Figure 4e). The high levels of *BMCC1* expression was significantly associated with young age ($P<0.00005$), favorable stages ($P<0.00005$), high expression of *TrkA* mRNA ($P<0.00005$), single copy of *MYCN* ($P<0.00005$), tumors found by mass screening (MS) ($P<0.00005$), nonadrenal origin ($P=0.0025$) according to the Student's *t*-test. The log-rank test showed that the high expression of *BMCC1* was significantly correlated with a favorable outcome ($P=0.0008$) as shown in the Kaplan–Meier cumulative survival curves (Table 1 and Figure 4f).

The multivariate Cox regression analysis also demonstrated that *BMCC1* expression (high vs low), age (<1 year vs ⩾1 year), *MYCN* copy number (1 copy vs >1 copy), and MS (positive tumors vs sporadic tumors) had prognostic significance ($P<0.0005$) (Table 2). *BMCC1* expression was significantly related to survival ($P=0.007$) after controlling age ($P=0.018$). However, it lost significance in a model including jointly with *MYCN* amplification or MS. Furthermore, *BMCC1* expression was significantly related to survival ($P=0.027$) after controlling age ($P=0.014$) and origin ($P=0.403$).

Changes in BMCC1 *mRNA expression during neuronal differentiation and apoptosis*

To examine whether exogenous expression of BMCC1 affects the cell growth of neuronal PC12 cells, a rat pheochromocytoma cell line, we transfected the cells with a full-length *BMCC1* cDNA. The overexpression of BMCC1 appeared to decrease the cell growth but the result was not statistically significant (data not shown). We then tested if expression of *BMCC1* mRNA was changed during neuronal differentiation and/or apoptosis. For that purpose, we used three different neuronal cell lines. The NT2 cell line, which was established from human immature teratocarcinoma and the cells show astrocytic differentiation after treatment with retinoic acid (RA) (Moasser *et al*., 1996). The CHP134 NBL cells undergo apoptosis after 3 days of the treatment with RA (Islam *et al*., 2000). On the other hand, the RTBM1 human NBL cells are induced to differentiate after the treatment with RA (Nakamura *et al*., 1998). We have confirmed that caspase 3 expression was increased in CHP134 cells but decreased in RTBM1 cells at day 7 after treatment with RA by semiquantitative RT–PCR. On the other hand, nestin expression was not changed in the former and slightly increased in the latter (Figure 5a). Expression of *BMCC1* mRNA was downregulated during RA-induced neuronal differentiation in both NT2 and RTBM1 cells, whereas it was rather upregulated in CHP134 cells on day 7 after the treatment with RA when many cells were undergoing apoptosis (Figure 5a).

To further confirm the above observation seen in neuronal cell lines, we examined the changes in *BMCC1* expression in superior cervical ganglion (SCG) neurons obtained from newborn mice in primary culture. The cultured cells were treated with 50 ng/ml NGF for 5 days (induction of neuronal differentiation) and then depleted NGF from the medium and added anti-NGF antibodies to induce neuronal apoptosis. As shown in Figure 5b, induction of differentiation by NGF decreased expression of *BMCC1*, whereas the NGF-depletion-induced apoptosis was accompanied with increase in *BMCC1* expression. This was very similar to the changes in expression of *c-jun* and *Bim* which had already been reported (Whitfield *et al*., 2001). Thus, the levels of *BMCC1* mRNA are changed during neuronal differentiation and apoptosis in an opposite manner.

Enhanced NGF-depletion-induced apoptosis in SCG neurons obtained from BMCC1 transgenic mice

We next generated *BMCC1* transgenic mice by using the expression construct with the tyrosine hydroxylase promoter-driven promoter to examine the functional role of BMCC1 in the sympathetic neurons. The SCG neurons obtained from either control or transgenic newborn mice were subjected to primary culture. The integration of the BMCC1 in the mouse genome and its overexpression in SCG neurons were confirmed by both

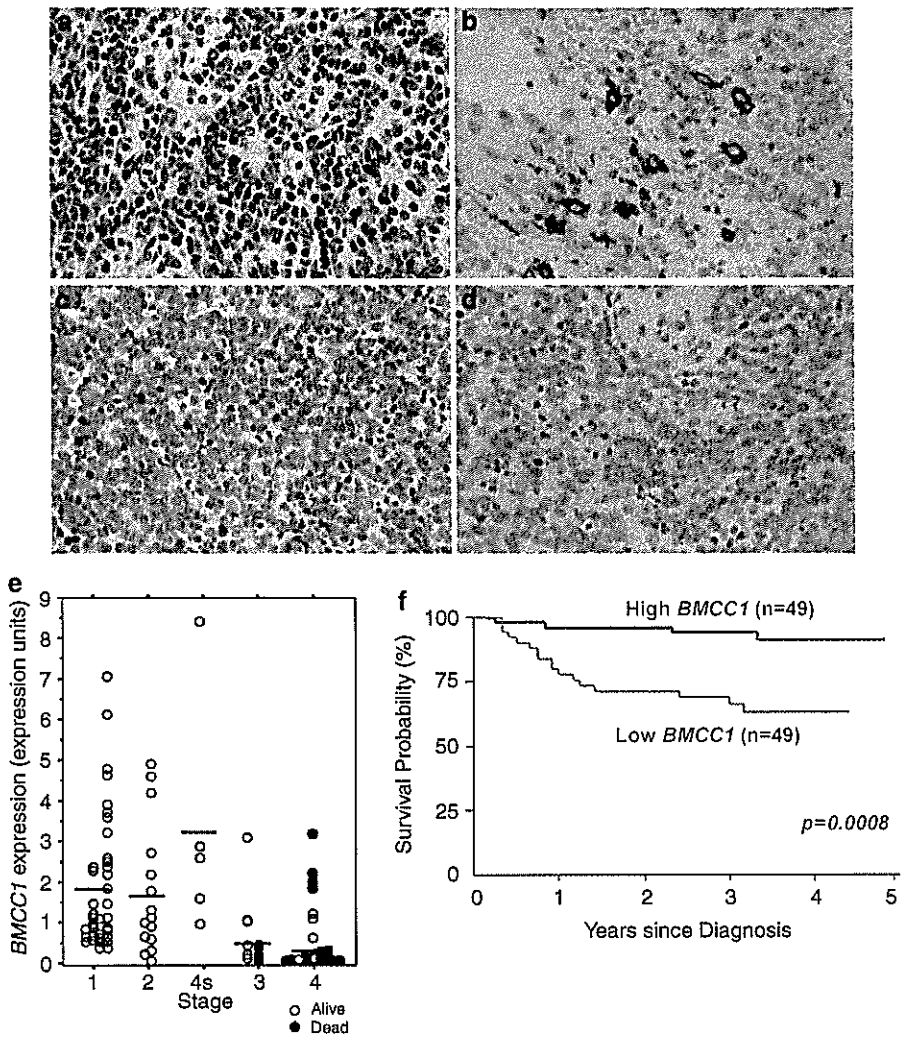

Figure 4 Immunohistochemistry and prognostic significance of BMCC1 expression in primary neuroblastomas. (**a**) and (**b**) In the favorable neuroblastoma without *MYCN* amplification, the tumor cells are occasionally positive for BMCC1 in the cytoplasm. (**c**) and (**d**) The unfavorable neuroblastoma with *MYCN* amplification is negative for BMCC1. (**a**) and (**c**) Hematoxylin–eosin staining. (**b**) and (**d**) BMCC1 immunostaining. (**e**) Low expression of *BMCC1* is associated with poor prognosis of the patients with neuroblastoma. Real-time quantitative RT–PCR analysis of *BMCC1* in 98 tumor samples from patients with neuroblastomas according to tumor stage. The levels of expression of *BMCC1* were normalized to that of *GAPDH*. Horizontal lines; group means, open circles; patients alive, solid circles, patients deceased. (**f**) Cumulative survival curves of patients with neuroblastoma, according to expression of *BMCC1* mRNA. The Kaplan–Meier curves show the probability of survival in terms of the level of expression of *BMCC1*. The survival curves were analysed by the Mantel–Haenszel log-rank test.

RT–PCR (Figure 6a) and Western blot (data not shown). The treatment of the transgenic SCG neurons with NGF in primary culture induced neurite extension similarly to control cells, but induction of apoptosis after depleting NGF was significantly enhanced in the cells overexpressing BMCC1 (Figure 6b–d). This suggested that BMCC1 overexpression may function as proapoptotic in neuronal cells.

Discussion

The presence of the highly conserved BCH domain in BMCC1 suggests its role in the regulation of apoptosis. BNIP2, which shares the BCH domain with BMCC1, has originally been identified as a molecule interacting with the adenovirus E1B 19-kDa protein. The E1B protein protects the cells from apoptosis induced by viral infection or other proapoptotic stimuli (Gooding *et al*., 1991; Hashimoto *et al*., 1991; White *et al*., 1992; Boyd *et al*., 1994). Bcl-2 and its related antiapoptotic proteins can functionally substitute for the E1B 19-kDa protein and bind to BNIP2. Therefore, it has been suggested that BNIP2 is a potential proapoptotic protein (Subramanian *et al*., 1995).

On the other hand, Cdc42 regulates the activation of the c-Jun amino-terminal kinase (JNK) in various cells (Bagrodia *et al*., 1995; Coso *et al*., 1995; Zhang *et al*., 1995). Cdc42 induces an apoptosis mediated by the JNK–MAP kinase cascade in Jurkat T lymphocytes (Chuang *et al*., 1997). The apoptosis is prevented by inhibitors of caspases, suggesting that activation of the

Table 1 Prognostic significance of *BMCC1* expression, age, stage, *TrkA* expression, *MYCN* amplification, mass screening and tumor origin in primary neuroblastomas (log-rank tests)

Variable	*t-tests*			*Log-rank tests*		
	Number of patients	*Mean±s.e.m. (BMCC1 exp.)*	P-*value*	*Number of deaths*	*Number of expected deaths*	P-*value*
BMCC1 expression						0.0008
Low	49			17	9.39	
High	49			4	11.61	
Age (year)						<0.00005
<1	63	1.82±0.23	<0.00005	5	14.55	
⩾1	35	0.64±0.15		16	6.45	
Tumor stage						<0.00005
1, 2, 4s	59	1.97±0.23	<0.00005	0	14.57	
3, 4	39	0.55±0.13		21	6.43	
TrkA *expression*						<0.00005
Low	44	0.91±0.22	<0.00005	21	7.75	
High	54	1.81±0.25		0	13.25	
MYCN *copy number*[a]						<0.00005
Amplified	27	0.30±0.10	<0.00005	18	4.14	
Single	70	1.80±0.20		3	16.86	
Mass screening						<0.00005
Positive	55	1.87±0.22	<0.0025	1	13.32	
Negative	43	0.80±0.22		20	7.68	
Origin						0.061
Adrenal gland	62	1.11±0.20	<0.00005	17	12.82	
Others	36	1.91±0.25		4	8.18	

[a]One patient who had missing *MYCN* information was excluded from analysis.

JNK pathway by Cdc42 is regulated by caspases. The interactive regulation between activation of JNK pathway and that of caspase cascade has also been reported in other biological systems (Cahill *et al*., 1996; Juo *et al*., 1997; Lenczowski *et al*., 1997; Seimiya *et al*., 1997). Cdc42 is also known to function as an initiator of neuronal cell death by activating a c-Jun-regulated transcriptional machinery (Bazenet *et al*., 1998). Cdc42GAP is a Cdc42-activating protein and, like Cdc42, binds to BNIP2 through the BCH domain when it is dephosphorylated at the tyrosine residue. Thus, the proteins with the BCH domain including BMCC1 seem to function in the regulation of apoptosis. The 'EYV' motif in the BCH domain, which is necessary for binding BNIP2 and Cdc42, is also conserved in the same domain of BMCC1. The role of P-loop in the regulation of apoptosis may also be important. Recently, it has been reported that ARTS (apoptosis-related protein in the TGF-β signaling pathway) mediates apoptosis through its P-loop motif. ARTS is a member of the septin family, localizes in cellular mitochondria and plays a role in regulating apoptosis. The P-loop consensus sequence is found in the proapoptotic protein, Apaf-1/CED-4 (Yuan and Horvitz, 1992; Zou *et al*., 1997; Larisch *et al*., 2000). It is interesting that BMCC1 also possesses a P-loop motif, also suggesting its proapoptotic function.

The biological importance of BNIP2 has been reported in the neuronal system. Expression of BNIP2 is developmentally regulated during the maturation of rat brain (Zou *et al*., 1997). The recent reports suggest that expression of *BNIP2* is downregulated by the treatment of NBL cells with estrogen (Garnier *et al*., 1997), and that both estrogen and progesterone promote survival of NBL cells through the BNIP2 function during the apoptosis induced by TNF-α (Vegeto *et al*., 1999). Furthermore, BNIP2 has been identified to be a putative downstream substrate of the FGF receptor tyrosine kinase signaling and possesses GTPase-activating activity to Cdc42. Thus, BNIP2 as well as Cdc42GAP seems to play a role in controlling the intracellular signals of neuronal differentiation and apoptosis.

However, our present results show that, among the molecules with the BCH domain, only *BMCC1*, but not *BNIP2* or *Cdc42GAP*, is differentially expressed among the NBL subsets, significantly at higher levels in favorable tumors than the aggressive ones. This suggests that *BMCC1*, rather than *BNIP2* or *Cdc42GAP*, is functioning *in vivo* in favorable NBLs undergoing neuronal differentiation and/or programmed cell death. The importance of *BMCC1* in NBL cell death has also been demonstrated in the study using neuronal cell lines. The RA-induced apoptosis of CHP134 NBL cells is accompanied with increased expression of *BMCC1*, while induction of differentiation in RTBM1 cells rather decreases its mRNA level. In the former system, the RA-triggered apoptosis induced upregulation of both

Table 2 Cox regression models using *BMCC1* expression and dichotomous factors of age, *MYCN* amplification, mass screening and tumor origin ($n=98$)

Model	*Variable*	P-*value HR (95% CI)*	*Variable*	P-*value HR (95% CI)*	*Variable*	P-*value HR (95% CI)*
A	*BMCC1* exp. (log)	<0.0005 0.53 (0.40, 0.70)				
B	Age (⩾1 vs <1 year)	<0.0005 7.5 (2.72, 20.7)				
C	*MYCN* (1 copy vs >1 copy)	<0.0005 0.035 (0.0099, 0.12)				
D	Mass screening (+ vs −)	<0.0005 0.028 (0.0037, 0.21)				
E	Origin (adrenal vs others)	0.072 2.7 (0.91, 8.08)				
F	*BMCC1* exp. (log)	0.007 0.55 (0.47, 0.89)	Age (⩾1 vs <1 year)	0.018 3.9 (1.26, 12.0)		
G[a]	*BMCC1* exp. (log)	0.72 1.05 (0.77, 1.47)	*MYCN* (1 copy vs >1 copy)	<0.0005 0.03 (0.0071, 0.13)		
H	*BMCC1* exp. (log)	0.079 0.77 (0.57, 1.03)	Mass screening (+ vs −)	0.003 0.04 (0.0053, 0.34)		
I	*BMCC1* exp. (log)	<0.0005 0.55 (0.41, 0.74)	Origin (adrenal vs others)	0.59 1.38 (0.42, 4.46)		
J	*BMCC1* exp. (log)	0.027 0.59 (0.49, 0.96)	Age (⩾1 vs <1 year)	0.014 4.1 (1.33, 12.9)	Origin (adrenal vs others)	0.403 1.5 (0.51, 5.32)

[a]One patient who had missing *MYCN* information excluded from the analysis. All variables were grouped into two categories, except *BMCC1* expression (log). HR, hazard ratio; 95% CI, confidence interval.

p21^{WAF1} and *caspase-3*, and downregulation of survivin. The downregulation and upregulation of *BMCC1* expression was also observed in the newborn mouse SCG cells undergoing NGF-induced differentiation and NGF-depletion-induced apoptosis in primary culture, respectively. Furthermore, in SCG neurons obtained from newborn transgenic mice for *BMCC1*, NGF-depletion-induced apoptosis was significantly enhanced. Thus, these results strongly suggest that *BMCC1* is stimulated or acts as a proapoptotic factor when the neuronal cell death is induced.

BMCC1 mRNA is induced at G1 phase of the cell cycle. The physiological significance of the cell cycle-dependent expression of *BMCC1* is currently unclear. However, activated Cdc42, a BMCC1-related molecule, also induces G1 cell cycle progression in quiescent Swiss 3T3 fibroblasts (Yamamoto *et al*., 1993; Olson *et al*., 1995) and upregulates E2F transcriptional activity in NIH3T3 cells to induce accumulation of cyclin D1 and hyperphosphorylation of RB protein (Gjoerup *et al*., 1998). BMCC1 may also play a role in G1-phase progression of the cell cycle via unknown mechanism.

Our statistical analysis has strongly suggested the importance of *BMCC1* expression in predicting the prognosis of NBLs. The *BMCC1* expression is upregulated in favorable NBLs and downregulated in unfavorable, advanced stages of NBLs. The similar pattern of expression in NBLs has also been reported in *TrkA* (Nakagawara *et al*., 1993, 1994; Nakagawara, 1998, 2001), *c-Ha-Ras* (Tanaka *et al*., 1998), *CD44* (Favrot *et al*., 1993) and *pleiotrophin* (Nakagawara *et al*., 1995). Here, we have added expression of BMCC1, at either mRNA or protein level, as a new prognostic indicator of favorable NBLs. Furthermore, our preliminary result has suggested that activated TrkA physically interacts with BMCC1, which in turn regulates the downstream signaling to control growth, differentiation and survival of neuronal cells (unpublished data). Therefore, BMCC1 could be a key regulator of TrkA-activation-mediated intracellular signaling pathway in favorable NBLs, that is defective in aggressive tumors such as those with *MYCN* amplification. Thus, BMCC1 might be an important molecular tool to develop new therapeutic strategy against aggressive NBLs.

Materials and methods

Patients

We studied tumors from 98 children with NBL which had been diagnosed between 1995 and 1999. In all, 55 patients were

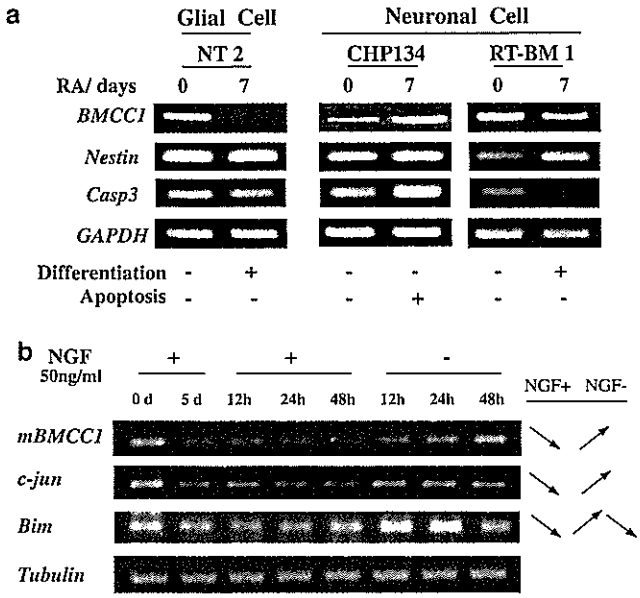

Figure 5 Expression of *BMCC1* during differentiation and apoptosis on neuronal cells. (a) The changes in *BMCC1* expression during induction of differentiation and apoptosis in neuronal cell lines. Two neuroblastoma cell lines (CHP134 and RTBM1) and teratocarcinoma cell line NT2 were treated with 5 μM all-*trans* retinoic acid (RA) or were cultured in the serum-free RPMI1640 medium for 7 days. Semiquantitative RT–PCR was performed using *BMCC1* primers and control *GAPDH* primers. (b) The changes in mRNA expression of mouse *BMCC1* during NGF-induced differentiation and NGF-depletion-induced apoptosis. Mouse superior cervical ganglion (SCG) cells were cultured with NGF for 5 days and were further cultured with or without NGF for indicated intervals (12, 24 and 48 h) (see Figure 6b, upper panels). *Tubulin* primers were used for standardization of the cDNA concentration for semiquantitative RT–PCR. *c-jun* and *Bim* were also used for positive controls.

identified by a MS program started in 1985. The selection of tumors for this study was solely based on the availability of a sufficient amount of tumor tissue, from which DNA and RNA could be prepared for the analyses described below. The diagnosis of NBL was confirmed by histologic assessment of the tumor specimen obtained at surgery according to the Shimada's classification (Shimada *et al*., 1984). The tumors were staged according to the International NBL Staging System (INSS) (Brodeur *et al*., 1993). In all, 39 tumors were stage 1, 15 stage 2, five stage 4, 10 stage 3 and 29 stage 4. The patients were treated according to the protocols previously described (Kaneko *et al*., 1998).

Tumor samples and cell lines

Fresh, frozen tumorous tissues were sent to the Division of Biochemistry, Chiba Cancer Center Research Institute, from various hospitals in Japan with informed consent from the patients' parents. All samples were obtained by surgery (or biopsy) and stored at −80°C. Studies were approved by the Institutional Review Board of the Chiba Cancer Center. Human cell lines which we used, except for COS-7, HEK 293 and HeLa cells, were cultured in the RPMI1640 medium (Nissui Pharmaceutical Co. Ltd, Tokyo, Japan) with 10% fetal bovine serum (FBS, Invitrogen Corp.) and 50 μg/ml penicillin/streptomycin (Invitrogen Corp.) at humidified 5% CO_2/95% air at 37°C. COS-7, HEK 293, and HeLa cells were grown in Dulbecco's modified Eagle's medium (DMEM) supplemented with 10% (v/v) FBS, 2 mM L-glutamine (Nissui Pharmaceutical Co. Ltd), 50 U/ml penicillin, and 50 μg/ml streptomycin.

Treatment of cell lines with RA

NT2, CHP134 and RTBM1 were seeded at a density of 1×10^6 cells per 10 cm tissue culture dish in the presence of 5 μM RA on the day of induction. The cells were grown for 7 days with substituting for culture medium with RA every other day. Total cellular RNA for preparing the RT–PCR templates was extracted after culturing for 7 days.

Cell cycle analysis

Approximately 50–70% confluent of HeLa cells were treated each by 400 μM mimosine for 18 h (G1 arrest), 2 mM thymidine for 20 h (S arrest), and 0.6 μg/ml nocodazole for 18 h (G2/M arrest). After confirmation of a synchronization of cultured cells by FACS, total RNA was extracted and the expression of *BMCC1* was examined by RT–PCR.

Northern blot analysis

Total RNA (25 μg) prepared from cell lines was electrophorased in 1% agarose-formaldehyde gels and transferred to a nylon membrane. For the hybridization probe, 1.5 kb fragment in 3′ part of *BMCC1* was used. Hybridization and washing were performed as described previously (Nagai *et al*., 2000).

Transfection and antibodies

Cells at 90% confluence in 60-mm plates were transfected with indicated plasmids using FuGENE 6 transfection reagent (Roche) for COS-7 and Lipofectamine 2000 reagent (Invitrogen) for HEK 293 cells according to their manufacturer's instructions. To generate the BMCC-1-specific antibody, rabbit antiserum was raised against the peptides individually (residues 31–59, 836–858, 993–1022, 1378–1402, 1719–1737, 2180–2209, 2693–2714) of human BMCC1. The antibody specific to C-terminal end of BMCC1 is crossreacted to human (transfectants), mouse (Neuro 2A) and rat (PC12) BMCC-1. Antiactin IgG (polyclonal) was purchased from Sigma, St Louis, MO, USA.

Semiquantitative RT–PCR

For semiquantitative RT–PCR analysis, 5 μg of total RNAs were converted to cDNA using random primers by Superscript II reverse transcriptase (Gibco-BRL). In all, 2 μl of the 100-fold dilution of cDNA was subjected to PCR. The 20 μl of PCR reaction mixture contained 1 μM forward and reverse primer specific for *BMCC1*, 250 μM deoxynucleotide triphosphates (dNTPs), 50 mM KCl, 10 mM Tris-HCl (pH 8.0), 1.5 mM $MgCl_2$ and 0.5 U Taq DNA polymerase (TAKARA, Otsu, Japan). The PCR amplification was carried out for 35 cycles (preheat at 95°C for 2 min, denature at 95°C for 15 s, annealing at 58°C for 15 s, and extension at 72°C for 20 s) in thermocycler (Perkin-Elmer Cetus, Foster City, CA, USA). The PCR products were electrophorased in 2.5% agarose gel, and visualized by UV illuminator. *BMCC1* primer sequences were as follows; forward: 5′-CGTTTATTTGCCGGTAGG AG-3′, reverse: 5′-GCTCAGGCTCTTTGGTAGGA-3′. As a control, *GAPDH* primers (forward primer; 5′-CTGCACCAA CAATATCCC-3′, reverse primer; 5′-GTAGAGACAGGG TTTCAC-3′) were also used with reduced cycle (28 cycles).

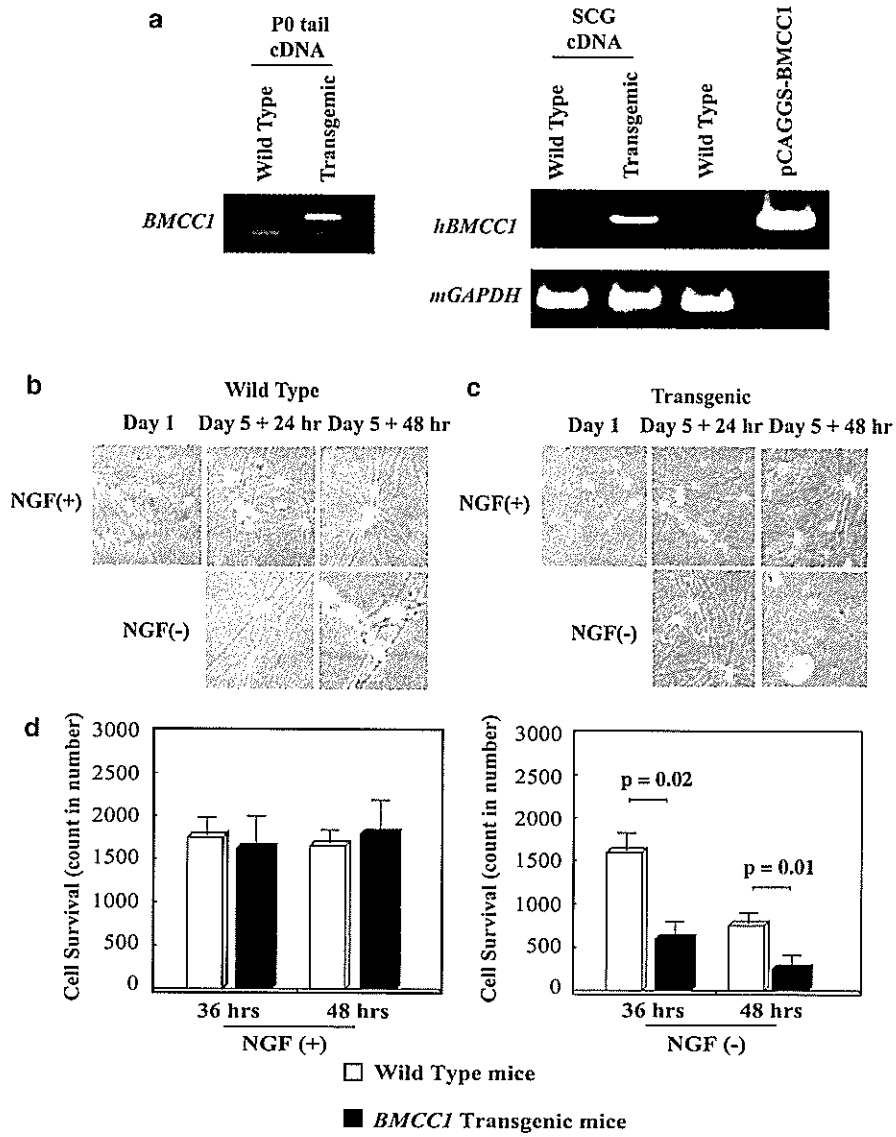

Figure 6 Increased apoptosis in superior cervical neurons obtained from newborn mice transgenic with the tyrosine hydroxylase promoter-driven human *BMCC1* in primary culture. (**a**) Expression of human *BMCC1* in SCG neurons obtained from *BMCC1* transgenic mice. SCG from both side of submandibular region was dissected from P_1 mice of wild-type and transgenic mice within 24 h after birth (described in Materials and methods). mRNA was purified from SCGs by using Trizol solution and RT–PCR was performed to confirm BMCC1 expression. Genotyping by PCR is shown in left panel. (**b**) and (**c**) Morphological changes in SCG neurons after treating with NGF and withdrawal of NGF. The SCG cells were obtained from wild-type (**b**) and BMCC1 transgenic (**c**) newborn mice. The cells were cultured in the presence of 50 ng/ml NGF for 5 days and were continuously treated with or without 50 ng/ml NGF for the following 2 days as described in Materials and methods. (**d**) Enhanced apoptosis in *BMCC1* transgenic SCG neurons after depletion of NGF. Numbers of survived SCG cells were counted at 36 and 48 h after NGF depletion. Values are shown as the means ± s.e.m. from triplicate cultures. Similar results were obtained in two additional independent experiments.

Quantitative real-time PCR analysis

For quantification of *BMCC1* in primary NBL, cDNA was synthesized with random primers by Superscript II reverse transcriptase (Gibco-BRL) from 15 μg of primary tumor total RNA. The following primers and probe were used; forward primer 5′-GGACAGTGGTCATTGGAGAACA-3′, reverse primer 5′-TTAGACCGTCCCCATAGTATCCTC-3′, probe 5′-FAM-ACATGAAGGTCATCGAGCCCTACAGG AGAG-TAMRA-3′. *GAPDH* primers and probes for control were purchased from Applied Biosystems. Quantitative real-time PCR analysis was performed by ABI7700 Prism sequence detector (Applied Biosystems), according to manufacturer's instructions using 1 × TaqMan Universal PCR Master Mix. After denaturing at 95°C for 10 min, PCR amplification followed by 40 cycles of denaturation at 95°C for 15 s and annealing/extension at 60°C for 1 min. A quantification of *BMCC1* mRNA in each samples was carried out by comparing with a standard curve, which was generated by reacting the plasmid containing *BMCC1*. Furthermore, *GAPDH* mRNA quantification was also performed for a standardization of the initial RNA content of each samples.

Exon prediction and bioinformatics

BLAST search against genome database revealed that 5′-region of *Nbla00219* was matched to the genome sequence of a

BAC clone RP11-146P9 (GenBank accession no. AL161625). We used GENESCAN algorithm (Burge and Karlin, 1997, 1998), and FGENESH algorithm (Solovyev and Salamov, 1999) to predict ORF from the genome sequence, and designed primers from each deduced exons. Using these primers and primers from 5′-region of *Nbla00219* cDNA, RT–PCR was performed to confirm the real exons. All PCR products were sequenced by the ABI automatic DNA sequencer (Perkin-Elmer Cetus) and resulting sequence were assembled to the full-length *BMCC1* cDNA. Bioinformatic analysis was performed using the PSORTII algorithm (Horton and Nakai, 1996), the SOPM algorithm and the TM pred algorithm against the predicted amino-acid sequences of *BMCC1*.

In situ *hybridization*
Section *in situ* hybridization was carried out as described previously (Takihara *et al*., 1997). The embryos were collected from pregnant females, and the morning the vaginal plug was detected was recorded as E0.5. A riboprobe was synthesized with digoxygenin-UTP and T3 or T7 polymerase (Roche Molecular Biochemicals). The alkaline phosphatase reaction was performed with NBT-BCIP (Roche Molecular Biochemicals). The riboprobes used for the section *in situ* hybridization were transcripts of the genomic DNA fragments of the *BMCC1* gene, a 835 bp PCR product of exon 3: the primers used are 5′-GAGATACTGGAGTTAGAAGAAG-3′ and 5′-TTCGGTCTTGGCTTTCTGGGTC-3′.

Immunohistochemistry
NBLs of favorable histology (Shimada system) without *MYCN* amplification and those of unfavorable histology with *MYCN* amplification were analysed. Anti-BMCC1 antibody was diluted to 1:50 and applied to the immunostaining. After deparaffinization, the sections were treated with 0.05% pronase solution for 5 min at room temperature. The biotin–streptoavidin method (Nichirei, Tokyo, Japan) was performed, and the reaction was visualized with diaminobenzidine solution.

Generation of BMCC1 transgenic mice
The full-length cDNA encoding human *BMCC1* was subcloned into the *Eco*RI site of the multicloning site region of the transgenic expression vector pCAGGS. The resulting plasmid, pCAGGS-*BMCC1*, was digested by *Alw44*I to isolate the transgenic cassette consisting of the CMV enhancer, the chicken *β-actin* promoter, the *BMCC1* cDNA, and the rabbit *β-globin* poly(A) sequence. The isolated region was purified for pronuclear injection into mouse embryos from FVB mice (Charles River Japan Inc.). Mouse embryos (fertilized one-cell zygotes) were injected and implanted in female CD-1 mice (Charles River Japan Inc.) at Japan SLC Inc. (Shizuoka, Japan). *BMCC1* transgenic mice were identified by slot blot analysis using genomic DNA prepared from mouse tails. *BMCC1*-positive founder transgenic mice then were backcrossed at least three times with C57BL/6 mice. Positive mice comprising the F_4 generation were subjected to SCG analyses.

Primary culture of newborn mice SCG cells
Primary cultures of sympathetic neurons were generated from dissociated SCG of postnatal-day 1 wild-type and transgenic mice as described previously (Lee *et al*., 1980). The cells were plated onto collagen-coated 24-well dishes at a density of around two ganglia per well and maintained in Modified Eagle's Medium supplemented with 10% heat-inactivated donor serum and 50 ng of mouse NGF per ml. A mixture of uridine and 5-fluorodeoxyuridine (10 μM each) was added on the following day to eliminate non-neuronal cells.

Statistical analysis
The Student's *t*-tests were used to explore possible associations between *BMCC1* expression and other factors, such as age. Since the values of the *BMCC1* expression were skewed, a log transformation was used to achieve the normality when using *t*-test and Cox regression. The distinction between high and low levels of *BMCC1* was based on the median value of the real-time PCR data (low, *BMCC1* <0.86 d.u.; high, *BMCC1* $\geqslant 0.86$ d.u.), regardless of tumor stage, *MYCN* copy, or survival. Kaplan–Meier survival curves were calculated, and survival distributions were compared using the log-rank test. Cox regression models were used to explore associations between *BMCC1*, age, *MYCN*, MS, origin and survival. Statistical significance was declared if the *P*-value was <0.05. Statistical analysis was performed using Stata 6.0. (Stata Corp. 1998. Stata Statistical Software: Release 6.0 College Station, TX: Stata Corporation).

Acknowledgements

We thank Shigeyuki Furuta, Shiho Hamano, Hiroyuki Inuzuka, Aiko Morohashi for technical assistance, Masayuki Fukumura, Toshihide Kanamori and Mika Kimura for helping full-length cDNA cloning, and Shigeru Sakiyama for encouragement. This work was supported in part by a Grant-in-Aid for the 2nd Term Comprehensive 10-Year Strategy for Cancer Control from the Ministry of Health, Labour and Welfare of Japan (AN), and by Grant-in-Aid for Scientific Research (B) (AN) and for Scientific Research on Priority Areas (2) 'Medical Genome Science' (MO, EI, AN) from the Ministry of Education, Culture, Sports, Science and Technology of Japan, and by a fund from Hisamitsu Pharmaceutical Co. Inc. (AN). We also thank following hospitals and departments for providing surgical samples: First Department of Surgery, Hokkaido University School of Medicine; Department of Pediatrics, National Sapporo Hospital; Department of Pediatric Surgery, Tohoku University School of Medicine; Department of Surgery, Gunma Children's Medical Center; Department of Pediatrics, Pediatric Surgery and General Surgery, Jichi Medical University; Department of Hematology and Oncology, Saitama Children's Medical Center; Department of Pediatrics, Juntendo University School of Medicine; Department of Surgery, Kiyose Metropolitan Children's Hospital; Department of Surgery and Pathology, Chiba Children's Hospital; Department of Pediatric Surgery, Chiba University School of Medicine; Department of Pediatric Surgery, Kimitsu Central Hospital; Department of Pediatric Surgery, Niigata University School of Medicine; Department of Pediatrics and Pediatric Surgery, Aichi Medical University; Department of Pediatrics, Kyoto Prefectural Medical University; Tumor Board, Hyogo Children's Hospital; Department of Pediatrics and Pediatric Surgery, Kagoshima University School of Medicine; Department of Pediatric Surgery, Showa University School of Medicine; Department of Pediatrics, Oita University School of Medicine; Department of Pediatric Surgery, Ohta General Hospital; Department of Pediatrics, Ichinomiya City Hospital; Department of Pediatric Surgery, Osaka City General Hospital; Department of Pediatrics, Nihon University School of Medicine Itabashi Hospital; Department of Pediatric Surgery, University of Tsukuba School of Medicine.